From Galactic to Extragalactic Jets: a Review

Jim Beall

Space Sciences Division,
Naval Research Lab, Washington, DC,

College of Science, GMU, Fairfax, VA,

And

St. Johns College, Annapolis, MD,

Astrophysics, like charity, begins at home:

This is a burlesque of an argument from Galileo's *Dialogue Concerning Two Chief World Systems*, where he compares the reflectance of surface of the Moon to the reflectance from a wall in sunlight.

Outline of Talk:

Jets are ubiquitous:

- star-forming regions
- galactic binaries and microquasars
- active galaxies and quasars
- clusters of galaxies

Association of jets with accretion disks

Association of jets in supernovae with GRB's

X-Ray Jet in the Radio Galaxy Pictor A

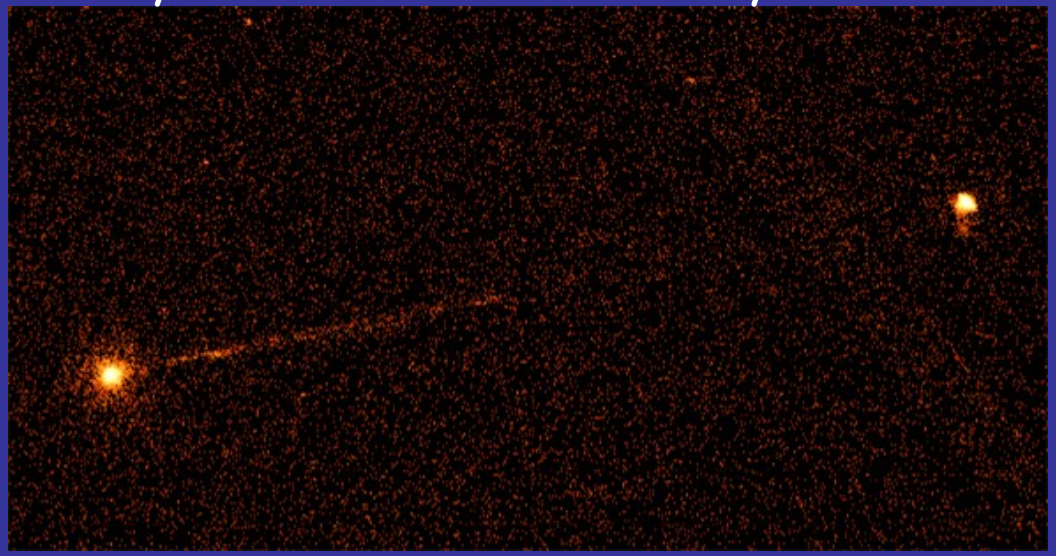

Crab Nebula (Chandra)

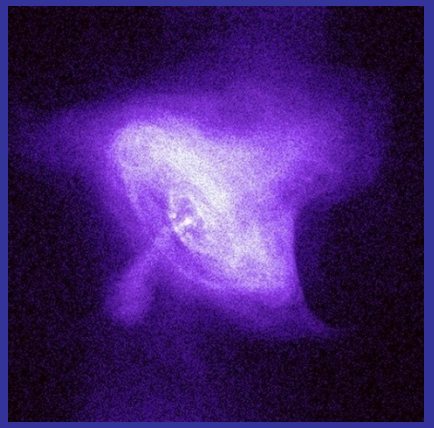

Vela Pulsar (Chandra)

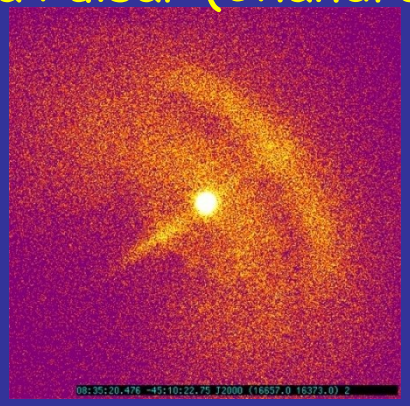

Cygnus A (Chandra)

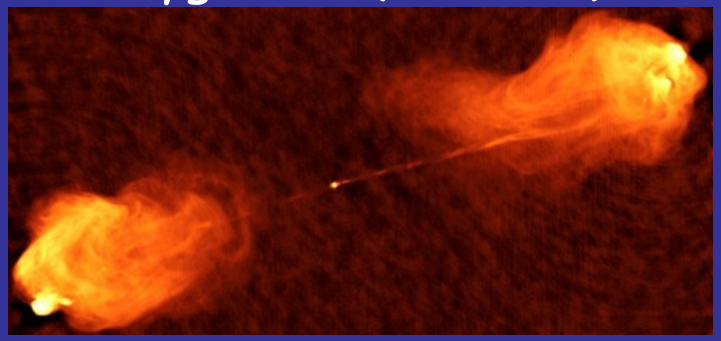

HH (Chandra)

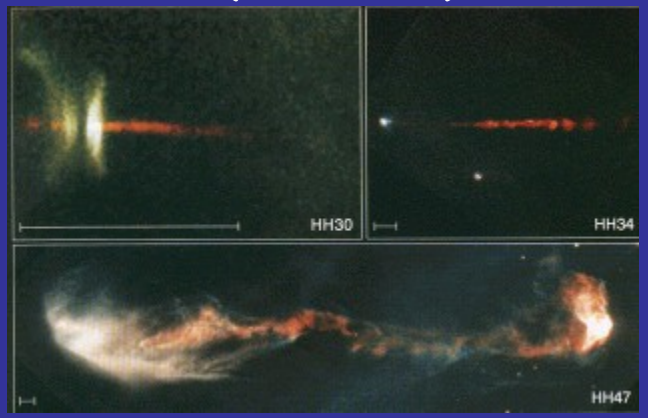

Cen A (Chandra)

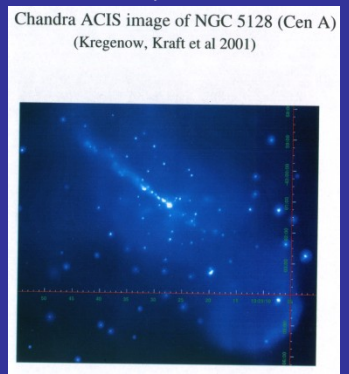

Comparison of Microquasars and Quasars (adapted from Mirabel)

AGN/Quasar Microquasar

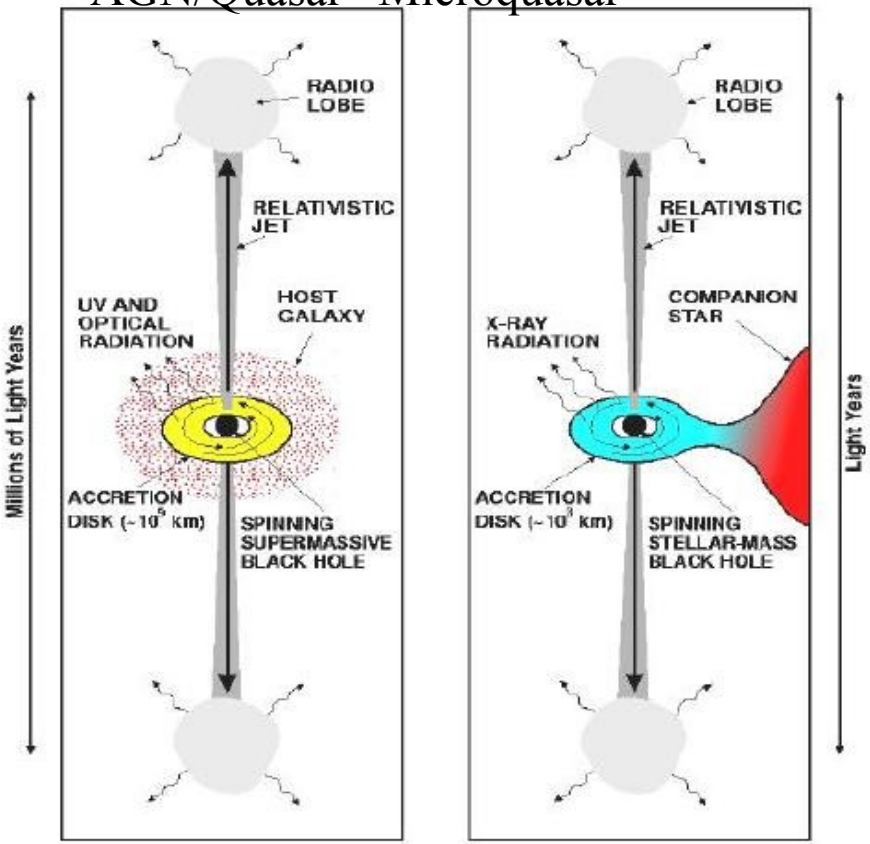

- Quasi-stellar relativistic object may be a Neutron Star or a black hole (BH)
- In BHs the scales of length and time are proportional to the mass of the BH
- The maximum color temperature of the accretion disk is $T_{col} \alpha (M/10M_{\odot})^{-1/4}$

ARE THERE BLACK HOLES WITH MASSES IN THE RANGE OF 10^2- $10^5 M_{\odot}$?

MICROQUASAR / QUASAR / GRB ANALOGY

(Yaël Fuchs, 2009)

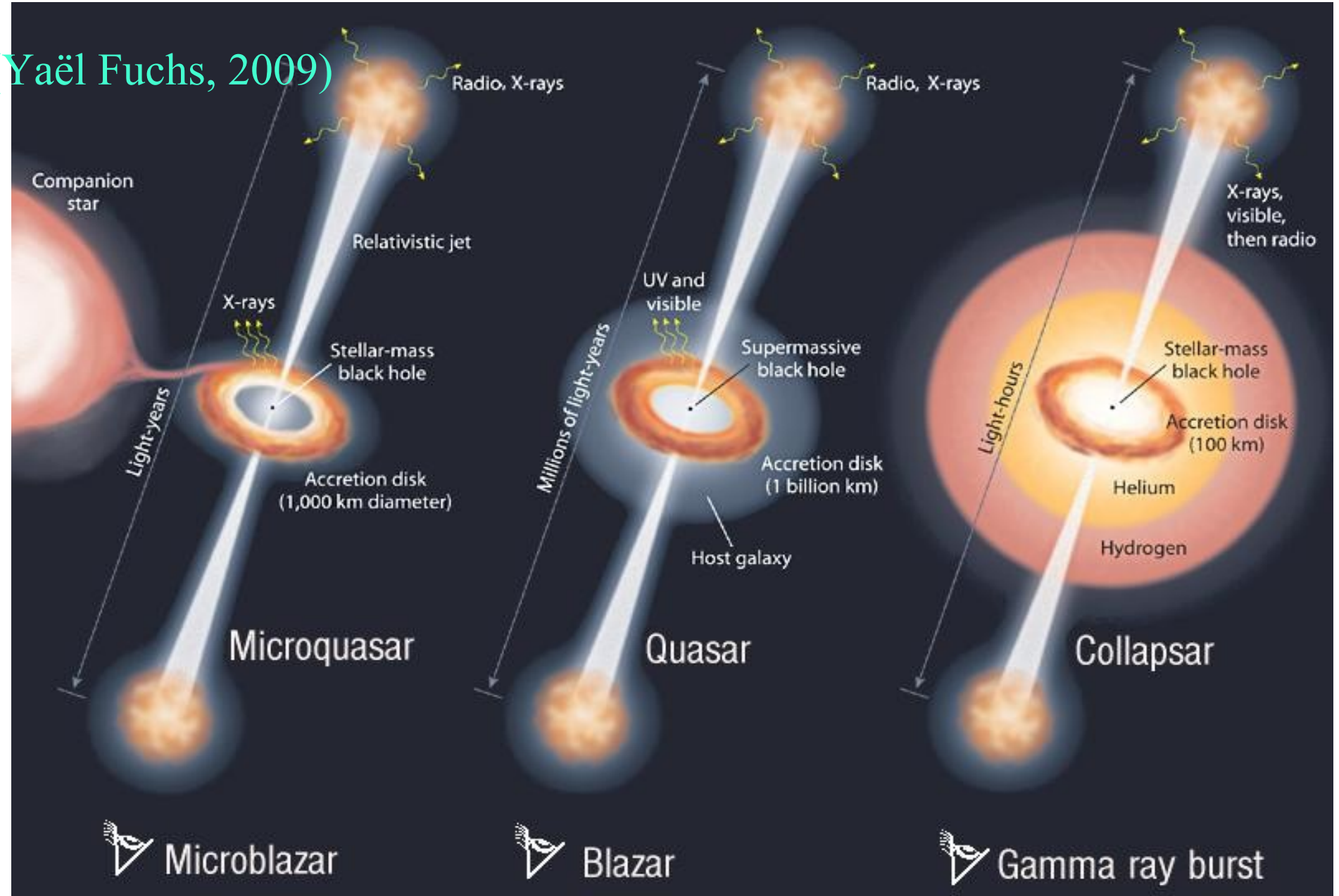

QUASARS MICROQUASARS

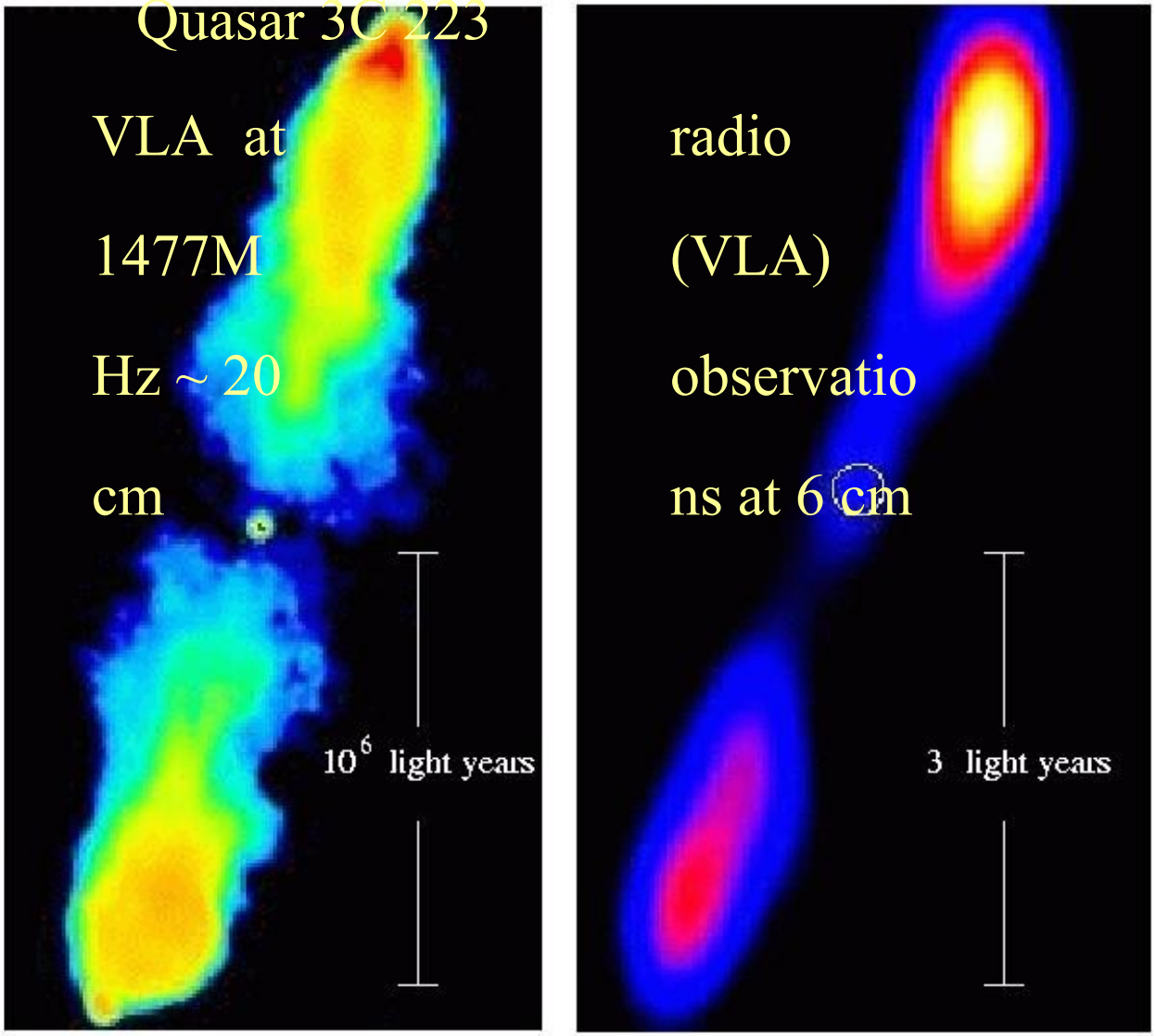

Jets in star-forming regions

Jets in Star-forming Regions in Molecular Clouds: There is evidence for accretion disks in the existence of bipolar outflows and in the agreement between calculated and observed spectra in giant molecular clouds. (see, ``The Observational Appearance of Protostellar Accretion Disks," in Beall 1987, Ap.J. 316, 227). Data on rho Ophiuchus taken from K. Tachihara's Ph.D. Thesis,

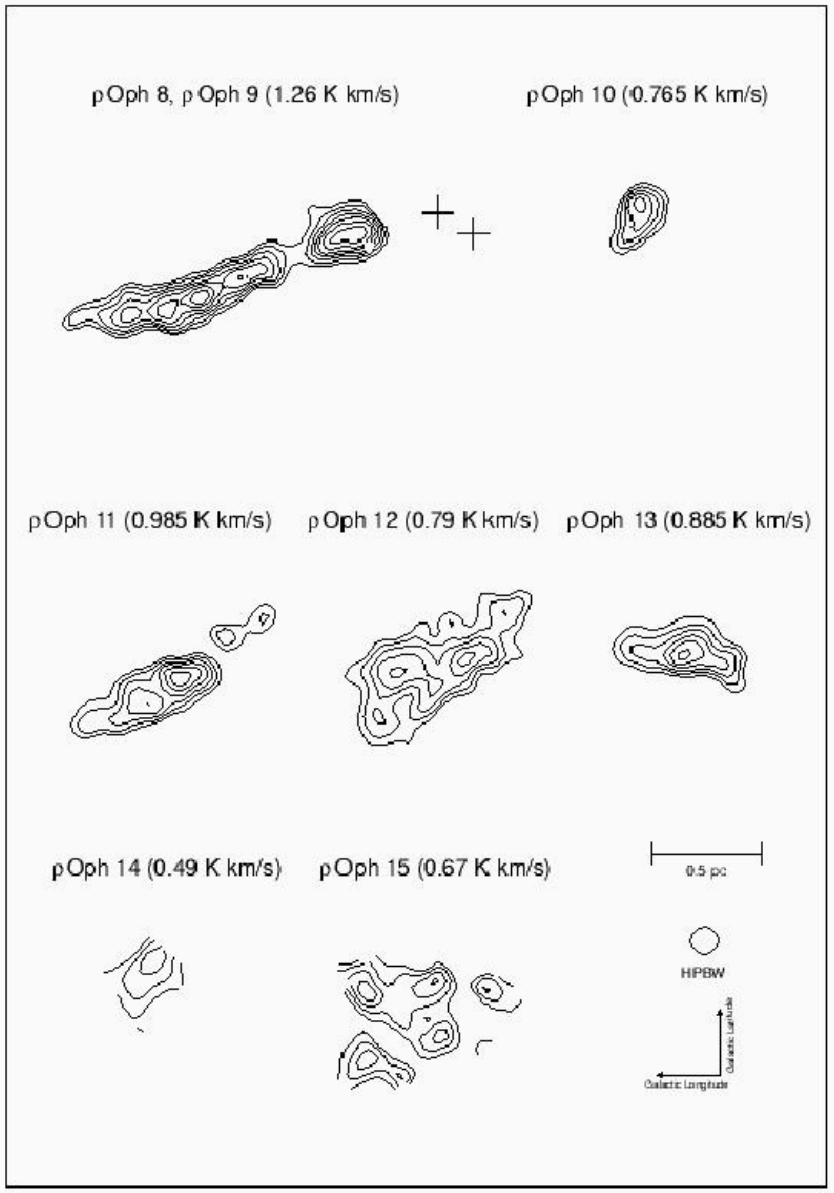

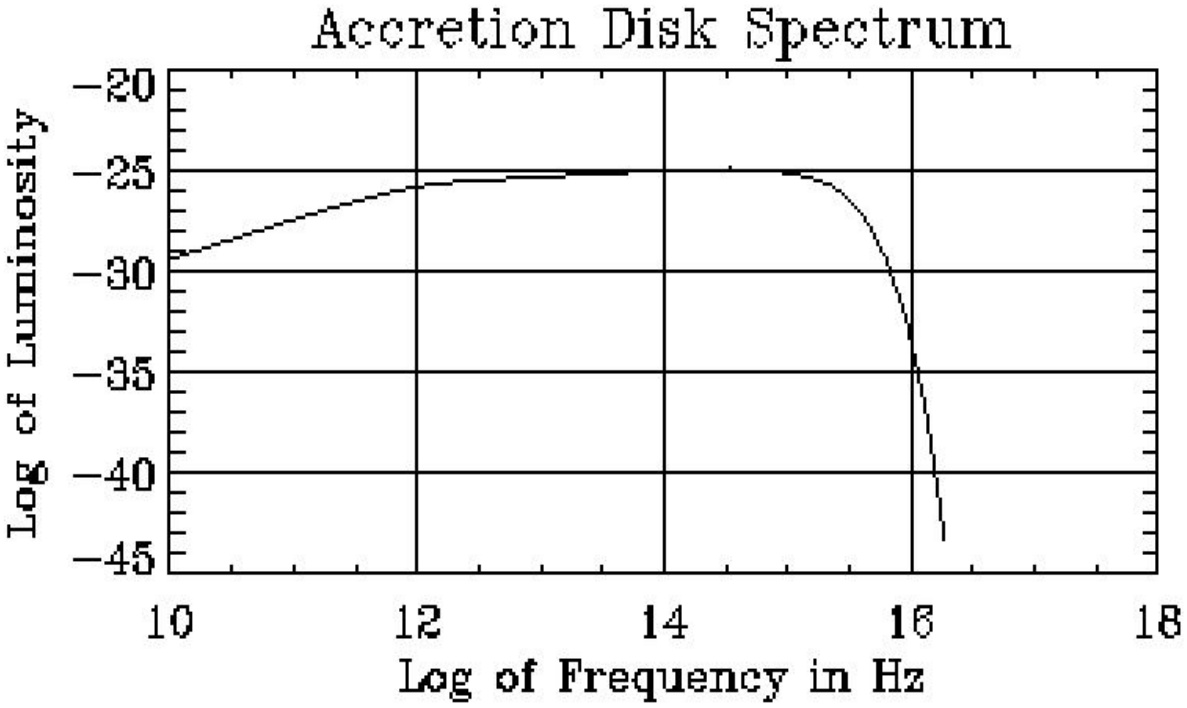

Calculation of accretion disk thermal spectrum (after Beall, J.H., 1987 ApJ, 316, 227), which showed that the rho Ophiucus cloud had IR spectra consistent with protostellar disks.

Thermal disk spectrum combined with Comptonized, soft x-ray photons upscattered to hard x-rays and gamma-rays (adapted from Hannikainen (2005)

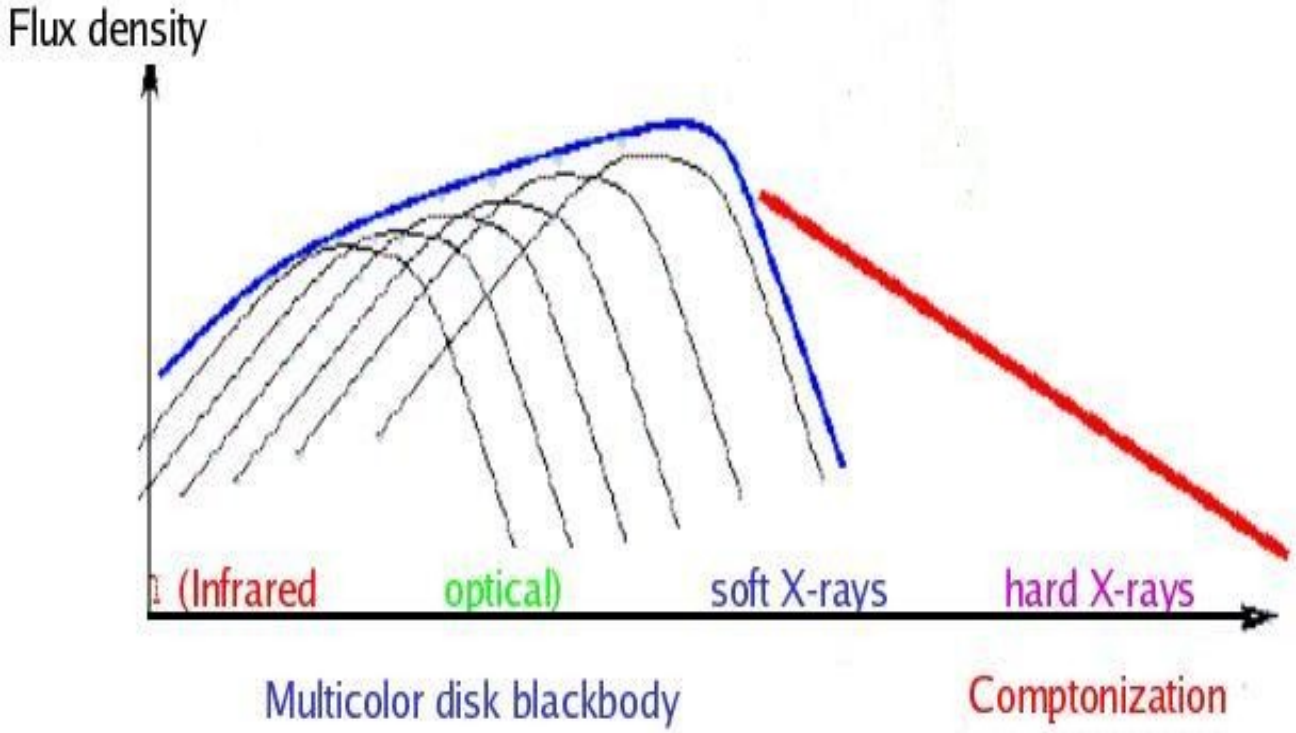

Mirabel 's discovery of superluminal jets in a galactic source (Mirabel and Rodriguez, Nature, 1994) obs of GRS 1915+105 (40,000 lt. years distant). Data taken from VLA observations.

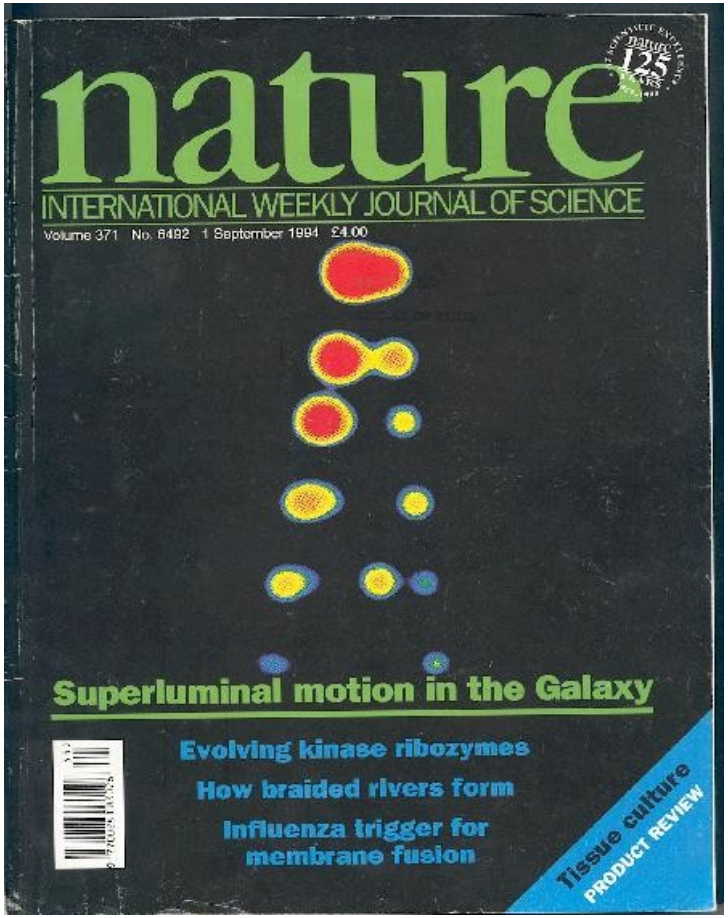

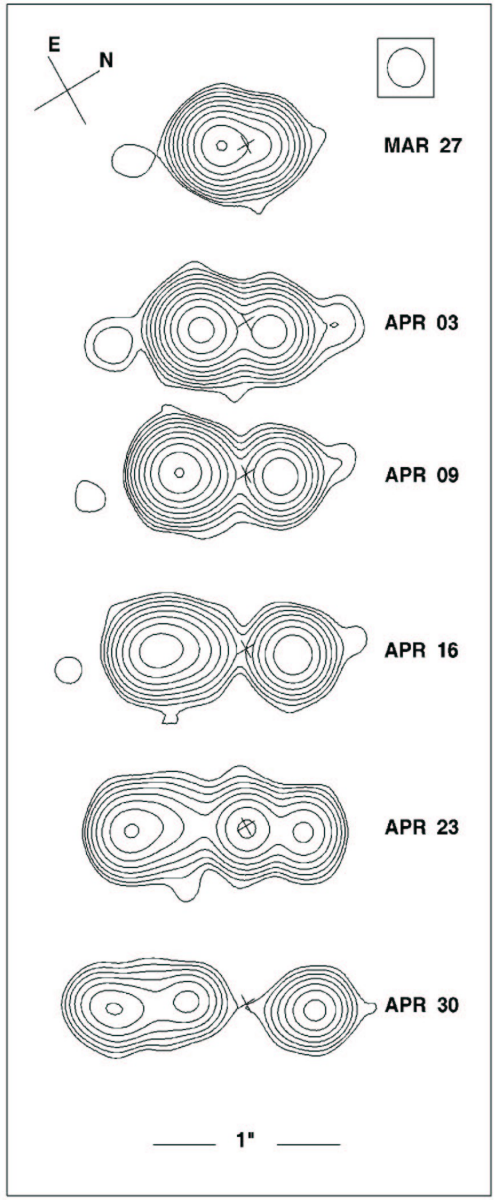

Galactic Microquasars show much the same behaviour as Quasars (after Mirabel)

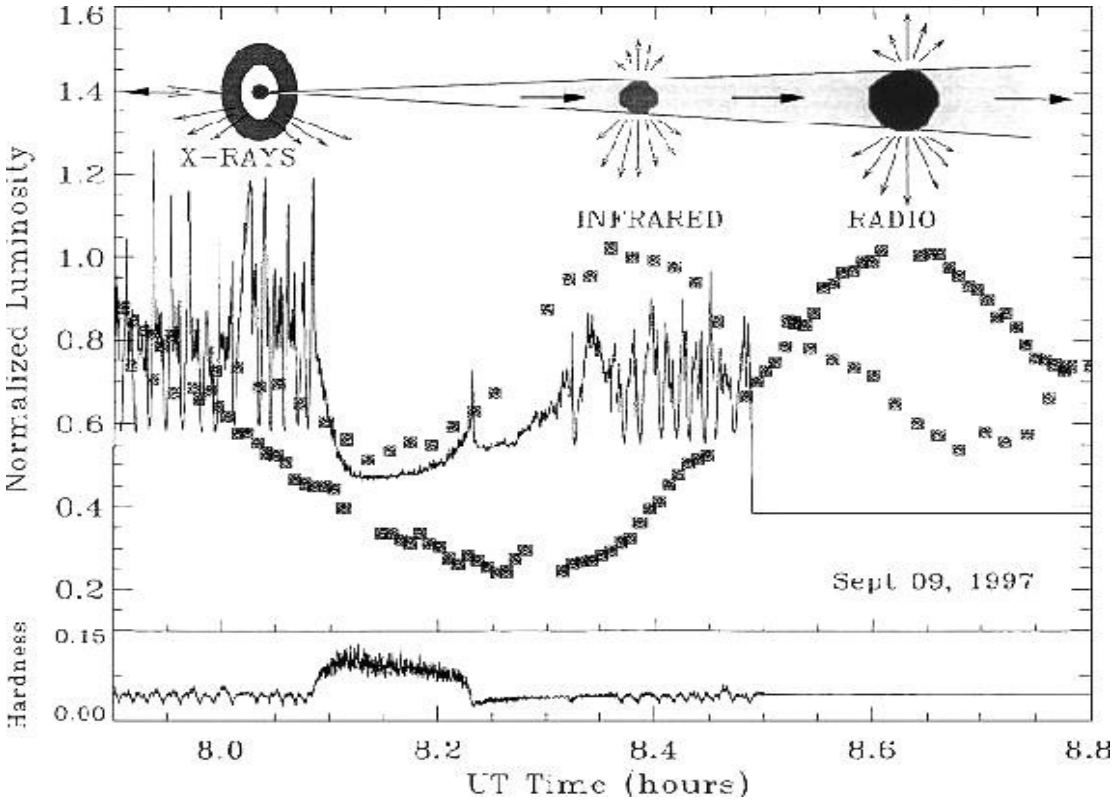

For GRS 1915 + 105, the radio peaks later than the infrared. Assuming that both come from the same synchrotron emitting volume, this is consistent with van der Laan expansion.

Synopsis of Variability Patterns

The data for the galactic microquasar (GRS 1915 + 105) are nominally consistent with van der Laan expansion.,

Sco X-1 frames from "movie" (see Fomalhaut, Geldzahler, and Bradshaw, 2001 Ap.J., 558, 283). For large "blobs", v = .45c. On this scale, 1 mas = 2.8 AU = 4.19×10^{13} cm with Sco X-1 at a distance, D = 2.8 Kpc (9000 light years).

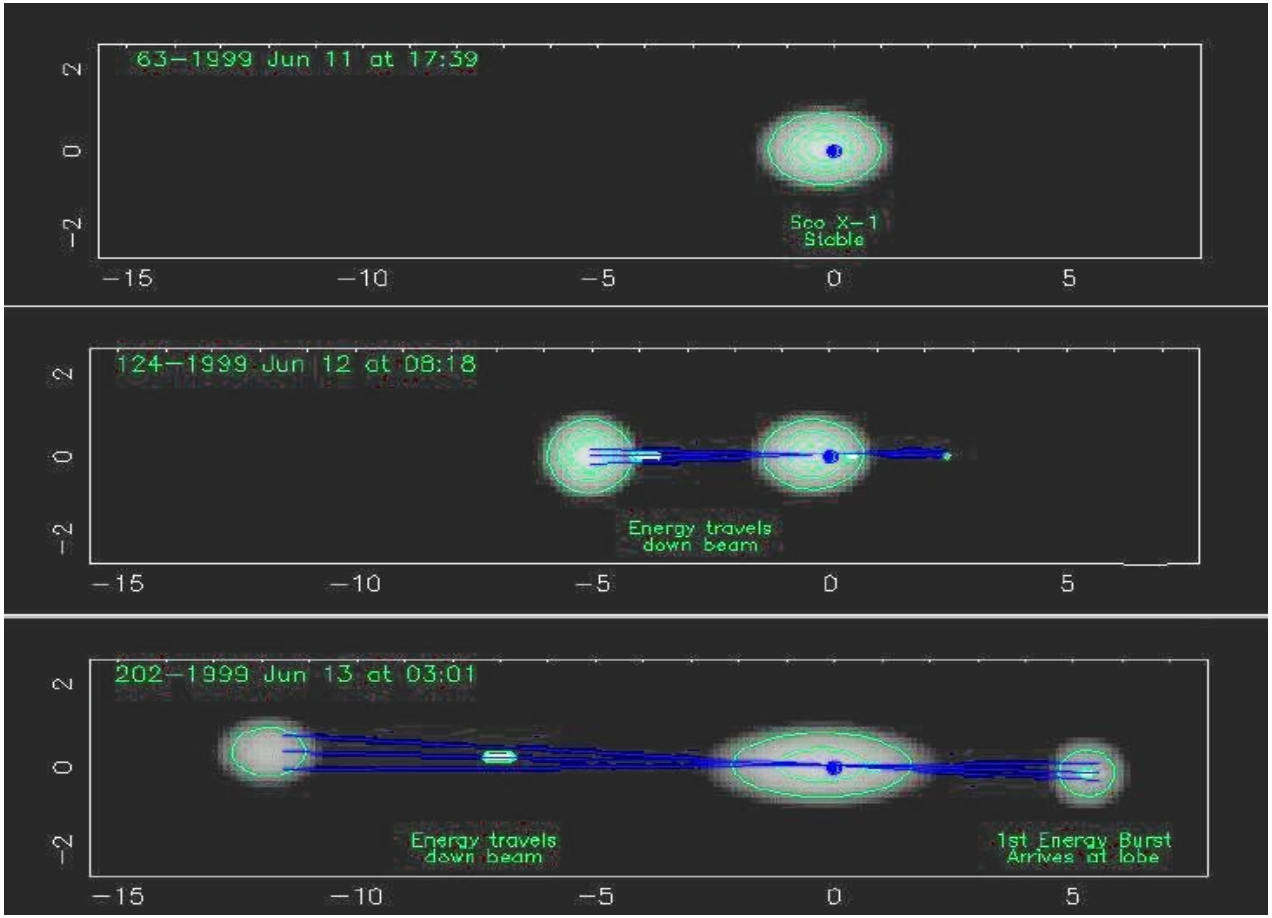

Sco X-1 frames from "movie" (see Fomalhaut, Geldzahler, and Bradshaw, 2001 Ap.J., 558, 283). For large "blobs", v = .45c. On this scale, 1 mas = 2.8 AU = 4.19×10^{13} cm with Sco X-1 at a distance, D = 2.8 Kpc (9000 light years).

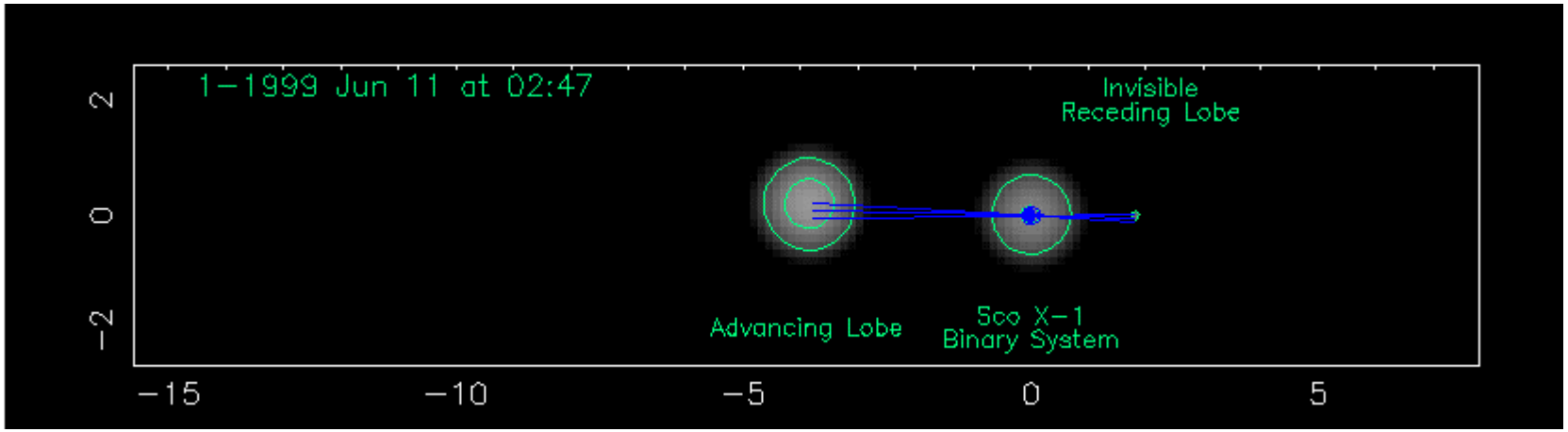

SS433 Observation from Hjellming and Johnston

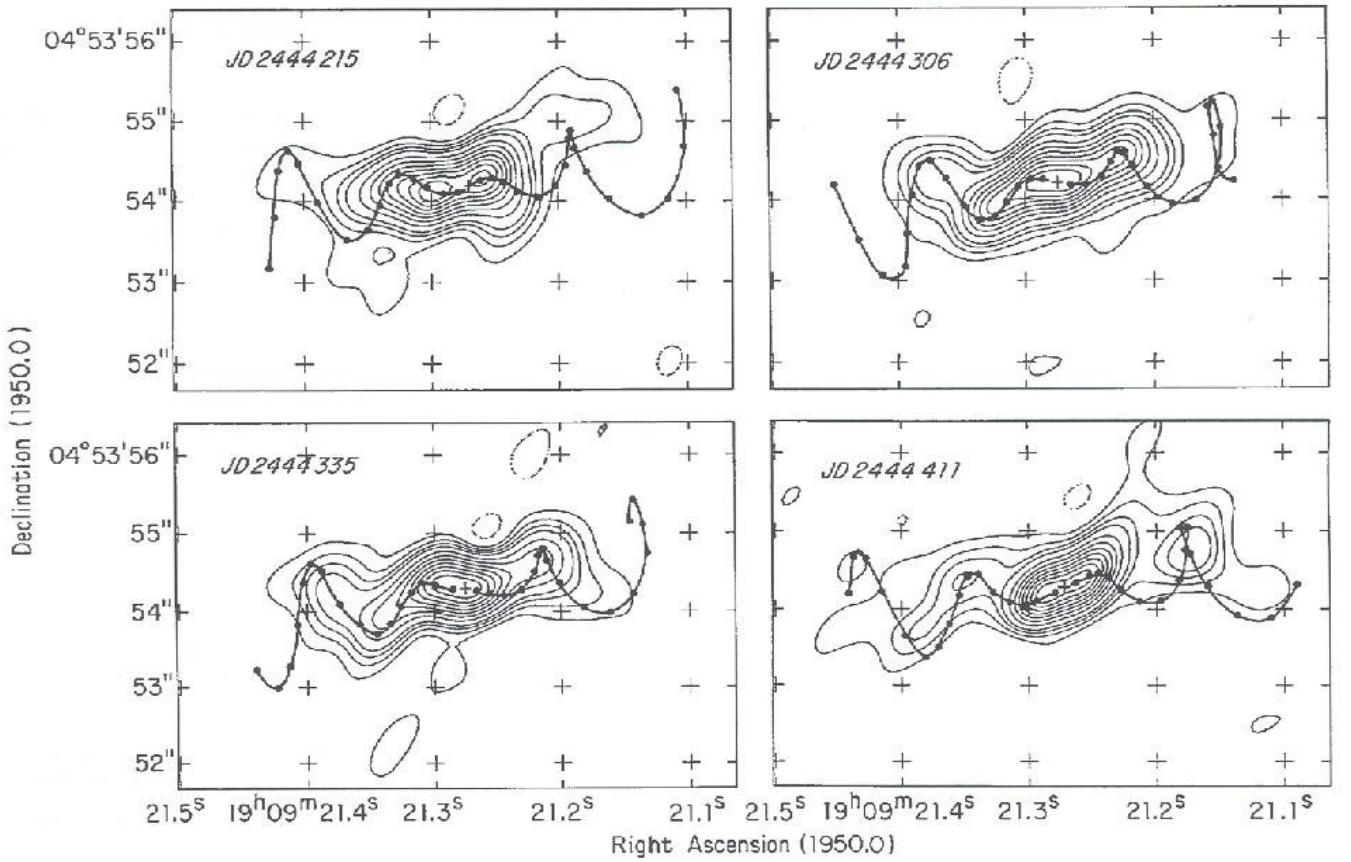

FIG. 2.—VLA radio contour maps of SS 433 at 4885 MHz for t=JD 2,444,215, 2,444,306, 2,444,335, and 2,444,111 are displayed in a form where the unresolved core radio source (small +) is removed, and the proper motion paths of material ejected at 20 day intervals with the parameters of Table 1 are drawn with filled circles. The contour levels correspond to 90, 80, 70, 60, 50, 40, 30, 20, 15, 10, 5, and −5% of the peak flux density values of 0.070, 0.030, 0.029, and 0.032 Jy per beam area for JD 2,444,215, 2,444,306, 2,444,306, and 2,444,411 maps, respectively.

SS433 VLBA observations (NRAO/MOJAVE)

Discovery of a High-Energy Gamma-Ray–Emitting Persistent Microquasar

Josep M. Paredes,[1*] Josep Martí,[2] Marc Ribó,[1] Maria Massi[3]

Microquasars are stellar x-ray binaries that behave as a scaled-down version of extragalactic quasars. The star LS 5039 is a new microquasar system with apparent persistent ejection of relativistic plasma at a 3-kiloparsec distance from the sun. It may also be associated with a γ-ray source discovered by the Energetic Gamma Ray Experiment Telescope (EGRET) on board the COMPTON–Gamma Ray Observatory satellite. Before the discovery of LS 5039, merely a handful of microquasars had been identified in the Galaxy, and none of them was detected in high-energy γ-rays.

High-resolution radio map of the nearby star LS 5039 obtained with the VLBA and the VLA in phased array mode at 6-cm wavelength.

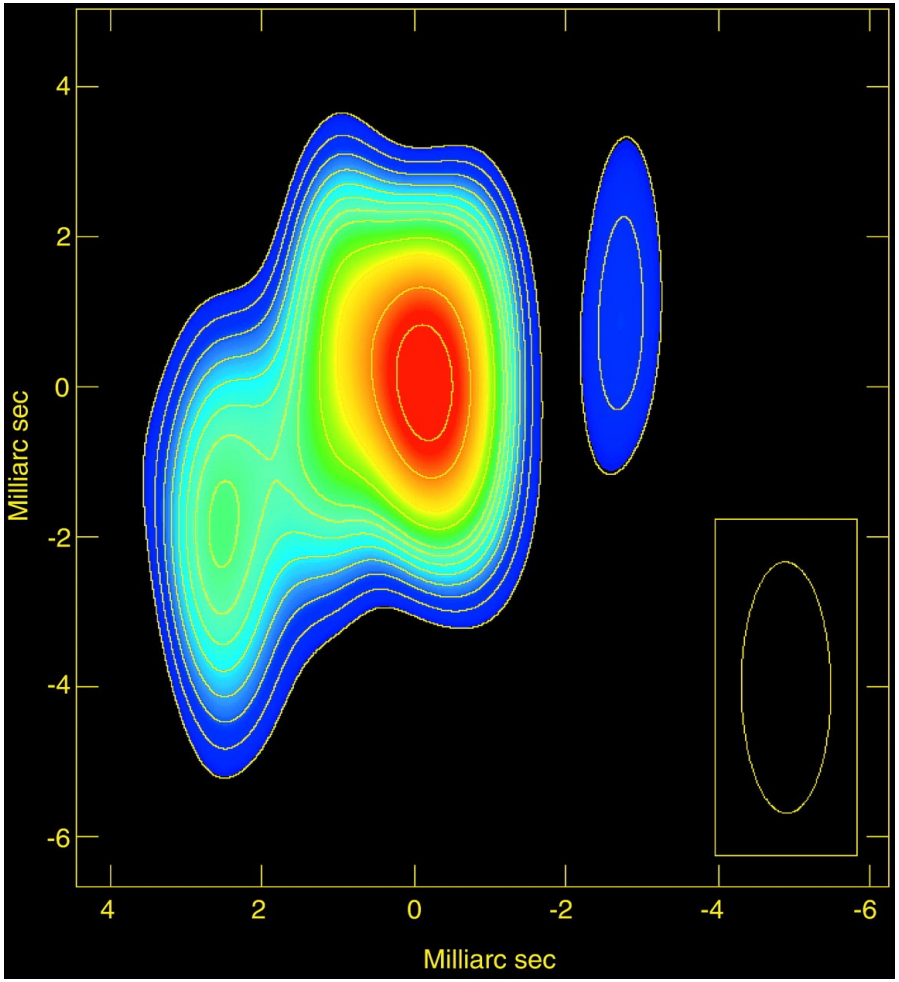

J M Paredes et al. Science 2000;288:2340-2342

Sketch of a Microquasar Binary System

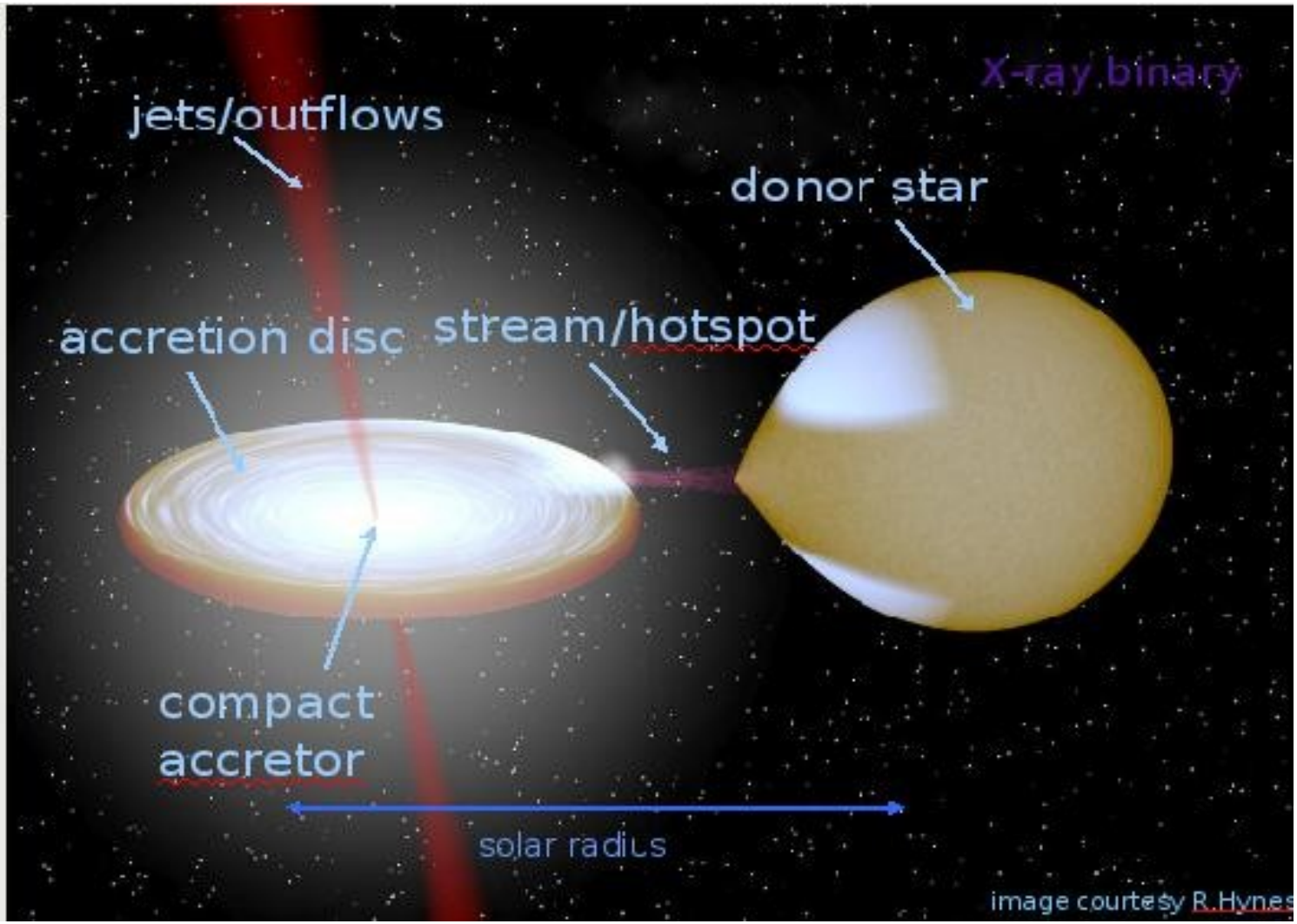

Multifrequency Image of M87 jet structure with arcsecond resolution instruments.

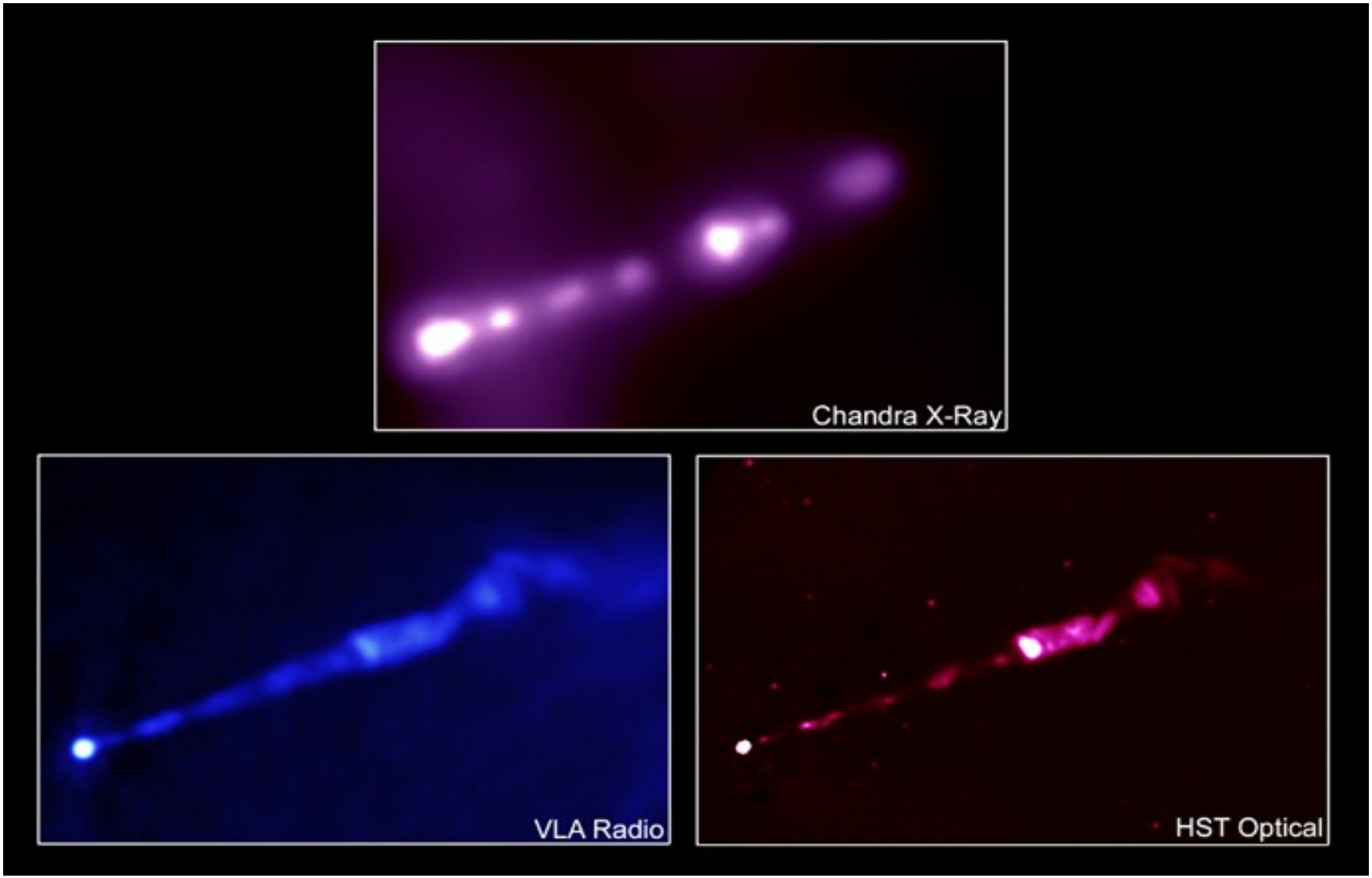

M87 at mas resolution (white bar is .01 pc)

Junor, Biretti, and Livio, Nature 1999, 401, 892

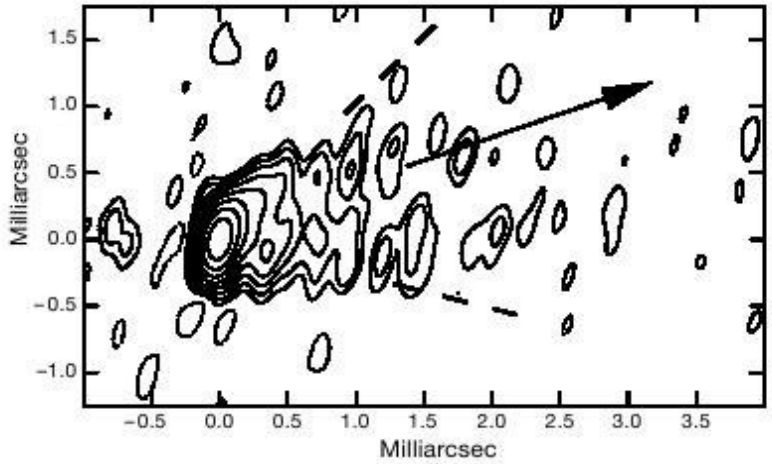

Figure 1 Image of the nucleus of M87 at 43.237 GHz on 3 March 1999. The synthesized beam is 0.33 mas × 0.12 mas (1 mas is 0.071 pc at the distance of M87) with the major axis in position angle −12.3°. The peak brightness in the image is 228 mJy per beam and the r.m.s. noise in the image well away from the bright structure is 0.38 mJy per beam. Contours are plotted at −1, 1, 2, 4, 8, 16, 32, 64 and 128 mJy per beam. The solid arrow indicates the direction of the 20″ jet, while the dashed lines indicate the position angles of the limb-brightened structure within 1 mas of the core. The antenna array consisted of the 10 telescopes of the Very Long Baseline Array (VLBA), 13 telescopes of the Very Large Array (VLA) phased together, and telescopes located at Effelsberg (Germany), Medicina (Italy), Metasahovi (Finland), Onsala (Sweden) and Yebes (Spain). Left circular polarization data were recorded at each telescope using 8 channels of 8 MHz bandwidth and 2 bit sampling. The data were correlated at the VLBA correlator, and later transferred to the AIPS package for calibration of the complex visibilities and imaging in a standard manner[25]. The complex visibility data have been weighted by the inverse fourth power of the signal-to-noise ratio of the complex visibility to improve the contribution of the higher spatial frequencies to the image.

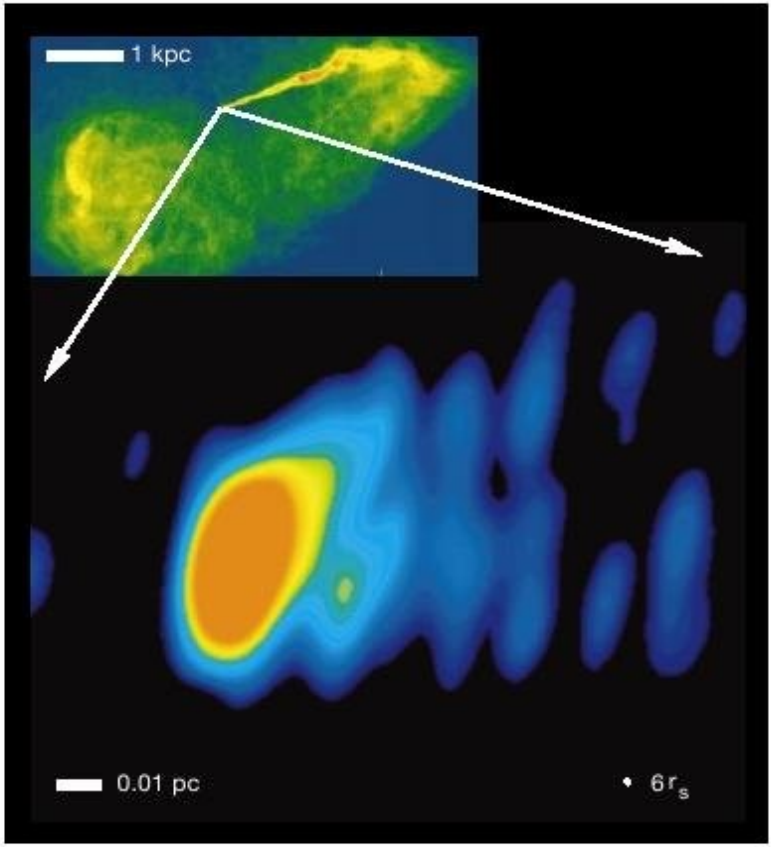

Figure 2 Pseudo-colour rendition of the nucleus of M87 at 43 GHz on 3 March 1999. See Fig. 1 for details. The filled white circle at lower right indicates $6r_S$, which is the diameter of the last stable orbit around a non-rotating black hole. The inset (top left) is a 15-GHz VLA image illustrating the large-scale jet.

Cen A radio and x-ray: resolution is also a critical consideration. See, e.g., H. Steinle's webpage at: http://www.mpe.mpg.de/~hcs/Cen-A/cen-a-home.html

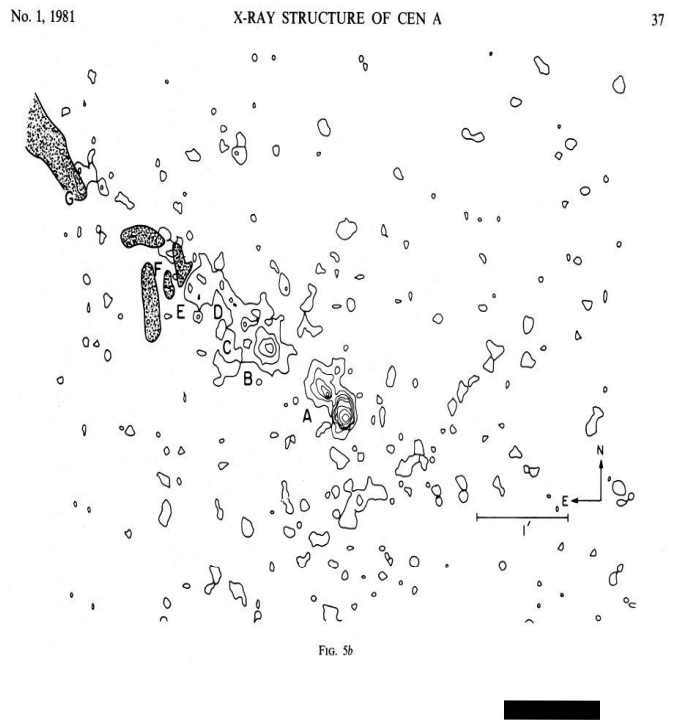

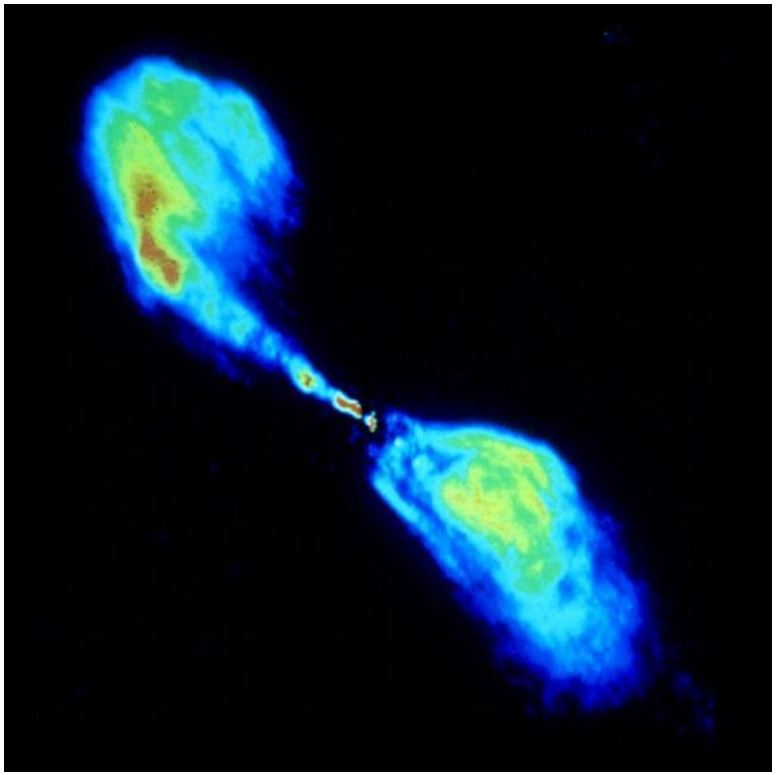

Feigelson et al. 1981: structure showing core + jet in x-ray. Bar ~ 1 arcminute

Burns and Price 6 cm. VLA image 1983, showing inner lobes (separated by 3.5 arcminutes).

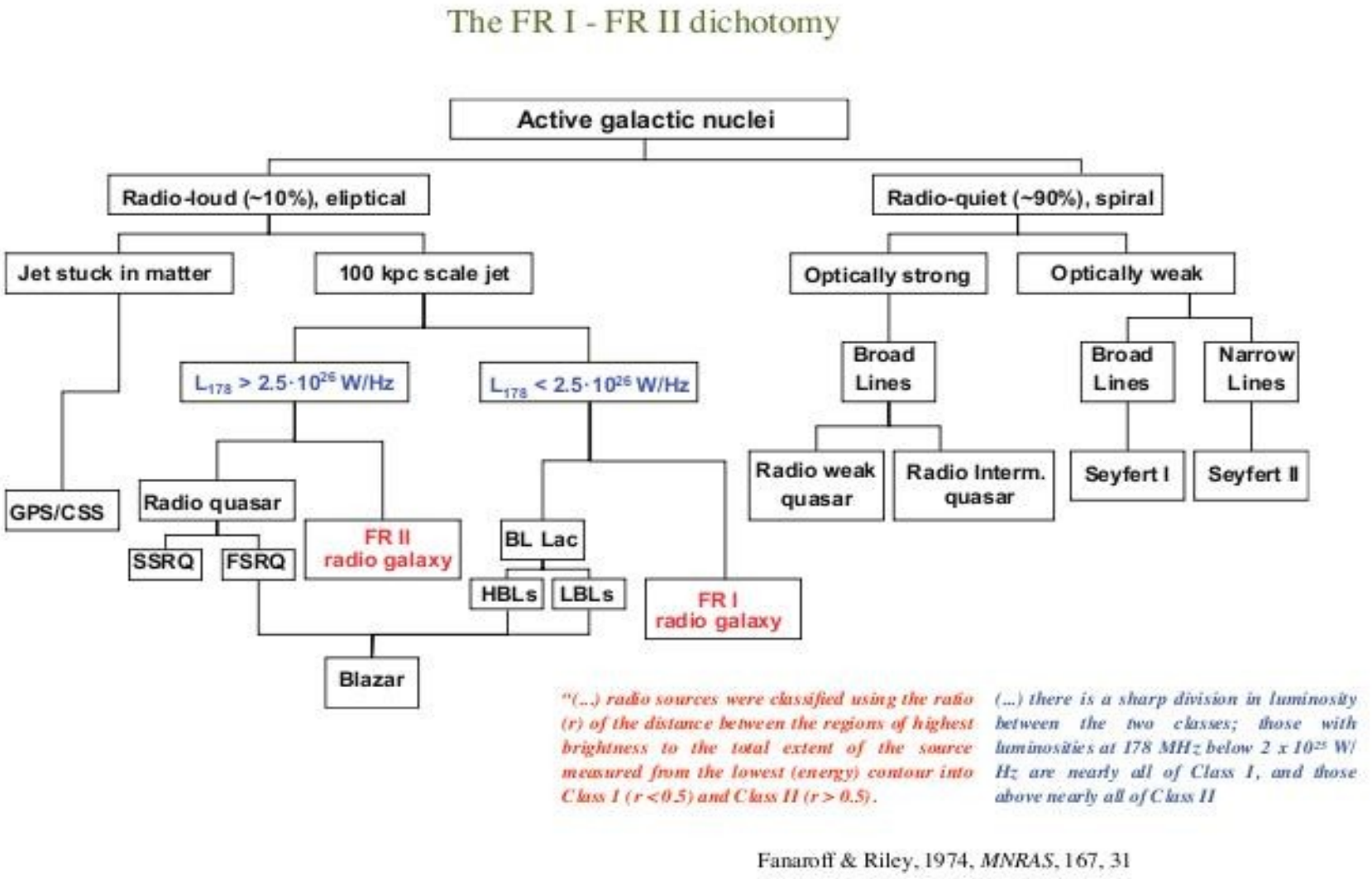

Courtesy of Paul Bordas (2011)

I will now focus on some canonical AGN jets in this part of the talk, partly from an historical view, and partly to consider some observations from Fermi and Swift that show the first concurrent optical, UV, IR, and γ-ray variability from Fermi (Bonning et al, 2009).

In the Late Jurassic (1968 through 1977), we conducted an investigation of the radio and x-ray variability of Cen A.

The work led to the first discovery of concurrent x-ray and radio variability of an AGN.

* Regarding the disk-jet connection, it is possible to get around the Eddington limit by more some multiple (see, e.g. Thomas Boller (2011), Nir Shaviv, 2011, Bozena Czerny (2012).

Low energy x-ray (2-6 keV) variability of Cen A

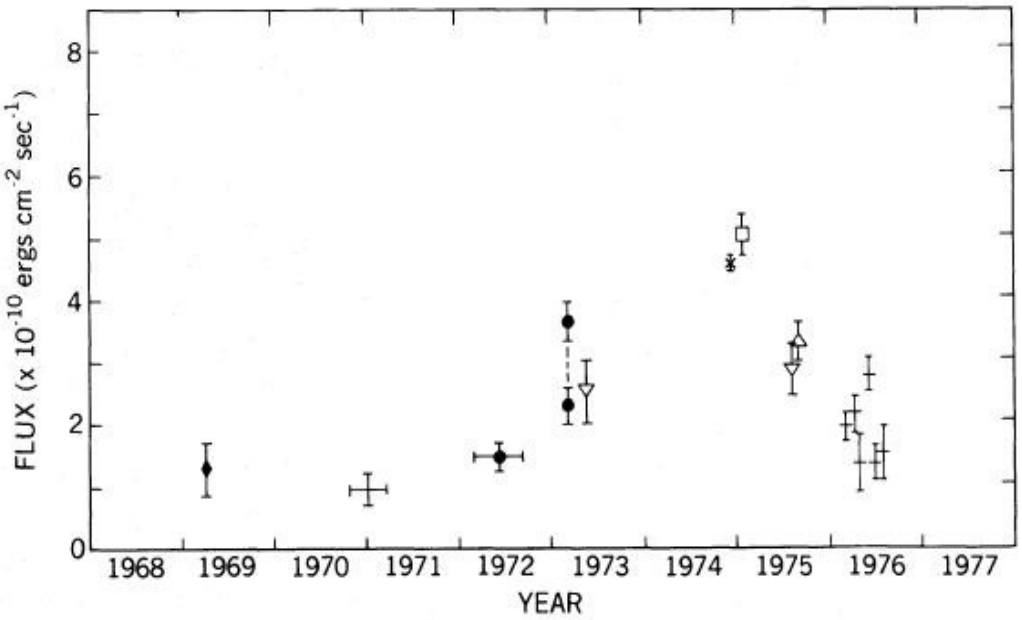

FIG. 2.—History of Cen A 2–6 keV X-ray flux. Data taken from Lampton *et al.* 1972, Tucker *et al.* 1973, Winkler and White 1975, Davison *et al.* 1975, Stark *et al.* 1976, Grindlay *et al.* 1975*b*, Serlemitsos *et al.* 1975, Sanford 1976.

Beall et al. 1978 Ap.J. 219, 836

High energy x-ray (~100 keV) variability of Cen A

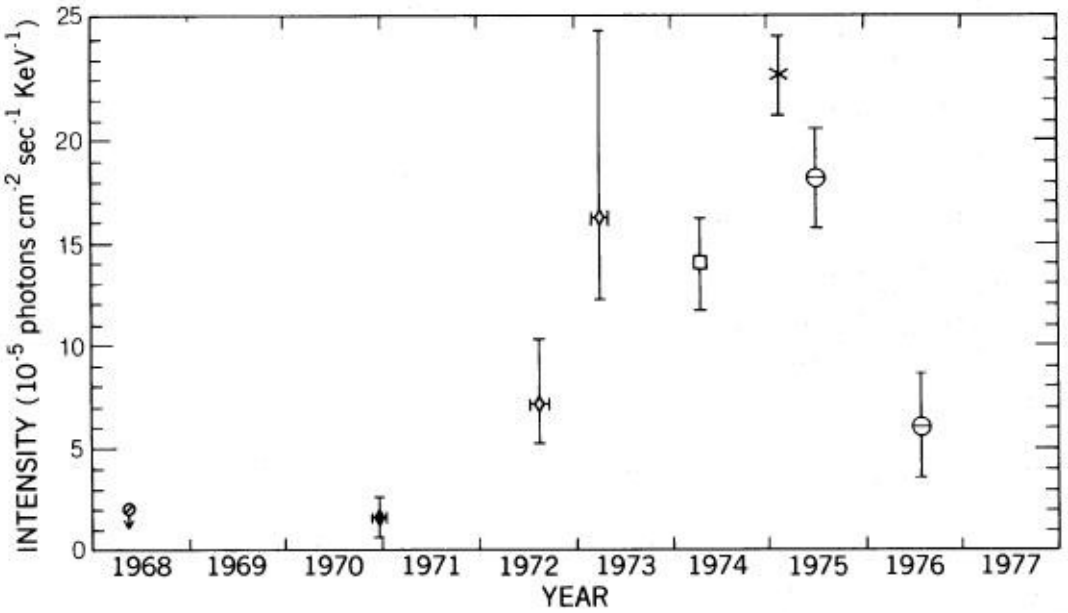

Haymes et al. (Balloon)=⊕; Lampton et al. (Balloon)=⧫; Mushotzky et al. (OSO - 7)=⊕;
Hall et al. (Balloon)=⊕; Stark et al. (Ariel V, Extrapolation)=⊗; Dennis et al. (OSO - 8)=⊕.

FIG. 3.—History of Cen A 100 keV X-ray intensity. Data taken from Haymes *et al.* 1969, Lampton *et al.* 1972, Mushotzky *et al.* 1976, Hall *et al.* 1976, Stark *et al.* 1976, and current observations.

Beall et al. 1978 Ap.J., 219, 836.

Historical radio variability of Cen A at 10.7, 31.4, and 90 GHz

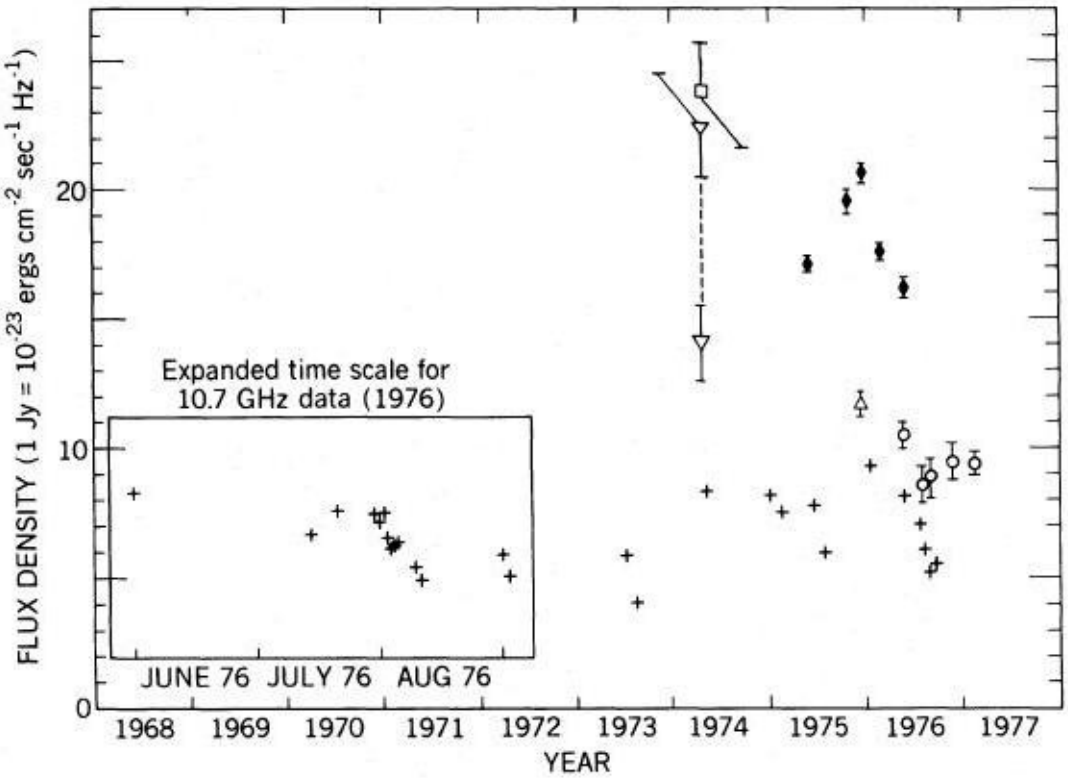

FIG. 1.—Radio emission from the nucleus of Cen A. Data taken from Price and Stull 1973, Stull and Price 1975, Dent and Hobbs 1973, Kellermann 1974, and current observations.

Beall et al. 1978 Ap.J., 219,836.

Historical spectral variability at 100 keV of Cen A

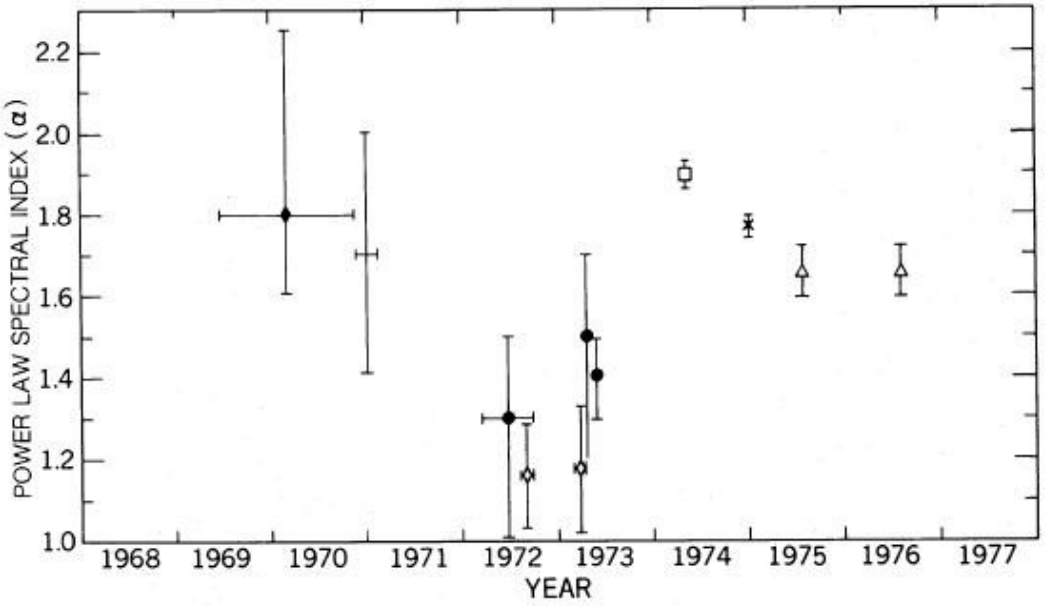

FIG. 4.—History of Cen A X-ray power-law spectral index. Data taken from Lampton *et al.* 1972, Tucker *et al.* 1973, Winkler and White 1975, Mushotzky *et al.* 1976, Hall *et al.* 1976, Stark *et al.* 1976, Mushotzky and Serlemitsos 1977, and current observations.

Beall et al. 1978 Ap.J., 219, 836.

Synopsis of Variability Patterns

The radio spectrum of the Cen A is consistent with a self-absorbed (at 10.7 Ghz) synchrotron emitting region and a power-law at higher radio frequencies. The x-ray data are consistent with either an SSC or Black-Body Compton or External Compton (EC) model. The hardening in the spectral index at the onset of the flare in 1972 suggests either an injection or re-acceleration of the source electrons.

This suggested that the source of the radio emission could be modelled by van der Laan (1966) expansion, where relativistic electrons are entrained in the magnetic field of a diffuse gas that was slowly expanding, with x-ray emission by an inverse Compton process.

Synopsis of Variability Patterns

But a careful look at van der Laan's paper shows that the Cen A data do not match the picture of an isotropic and isotropically emitting source consistent with van der Laan expansion because of the second radio flare from mid 1975 to mid 1975, which has no accompanying x-ray flare.

It appears we have observed a very complex interaction of a new plasmon or jet interacting with the environment in the AGN core.

Feigelson et al (1981) observed the source with ROSAT, and saw a linear structure, one-sides, that was along the radio-lobes-Cen A-center axis, but that structure is too distant to be the (supposed) recently created jet.

For the Cen A data, it was the **concurrent variability** that suggested the radio and x-ray fluxes were created **in the same region**. This suggested we could get **source parameters** from **observations + models:**

1. Synchrotron radiation for radio sources
2. Optical and infrared from thermal sources
3. X-ray and high-energy x-rays from SSC (synchrotron self-Compton) and external or BBC (blackbody Compton)
4. Gamma-ray production from multiple self-Compton scattering or hadronic processes (see e.g. Dar and Loar, 1997, Beall and Bednarek 1999, and Purmohammad and Samimi, 2001).
5. Neutrino production from hadronic interactions

Synopsis of Variability Patterns (continued)

Although in a narrower range of frequencies, the data for 3C 454.3 show concurrent variability in the γ-ray and optical, and a suggestive lag in the IR bands.

3C 454.3 Concurrent Variability: Fermi and Swift Data

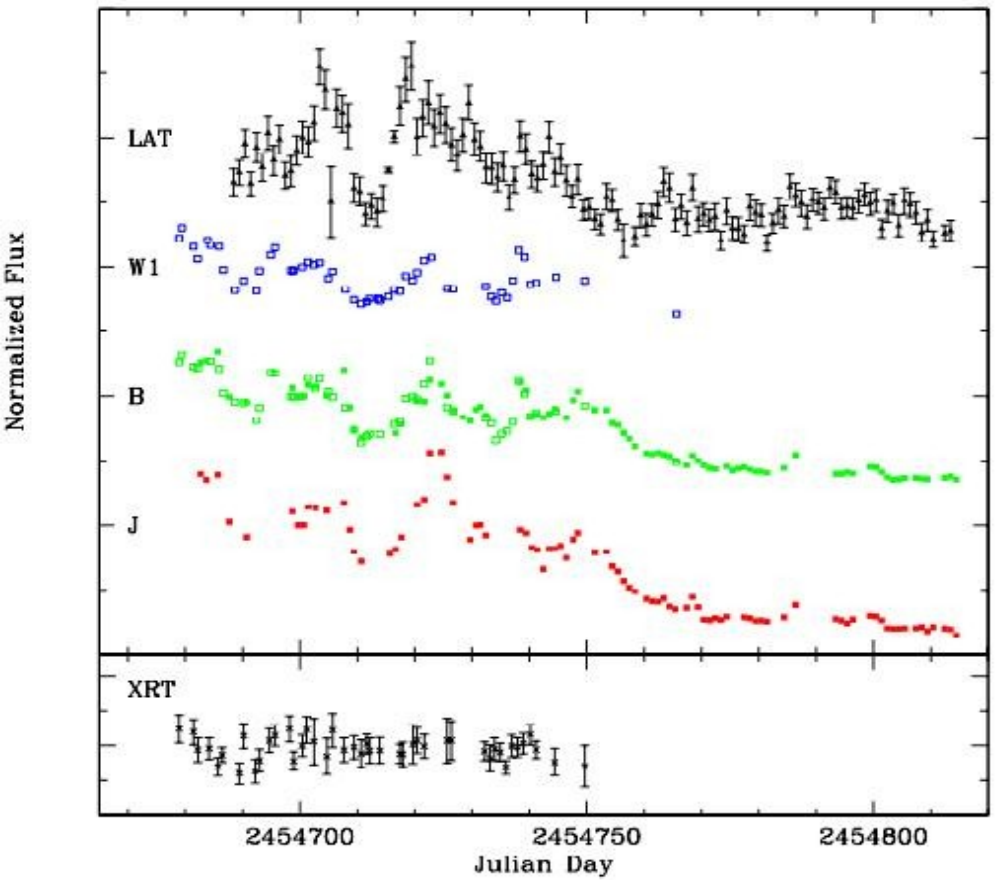

Variability of 3C 454.3 Fermi 0.1 – 300 GeV gamma-ray, UV (W1), optical (B),and IR (J) , and x-ray (XRT), taken from Figure 1, Bonning et al. 2008, ApJ (arXive:0812.4582v1)

3C 454.3 Concurrent Variability

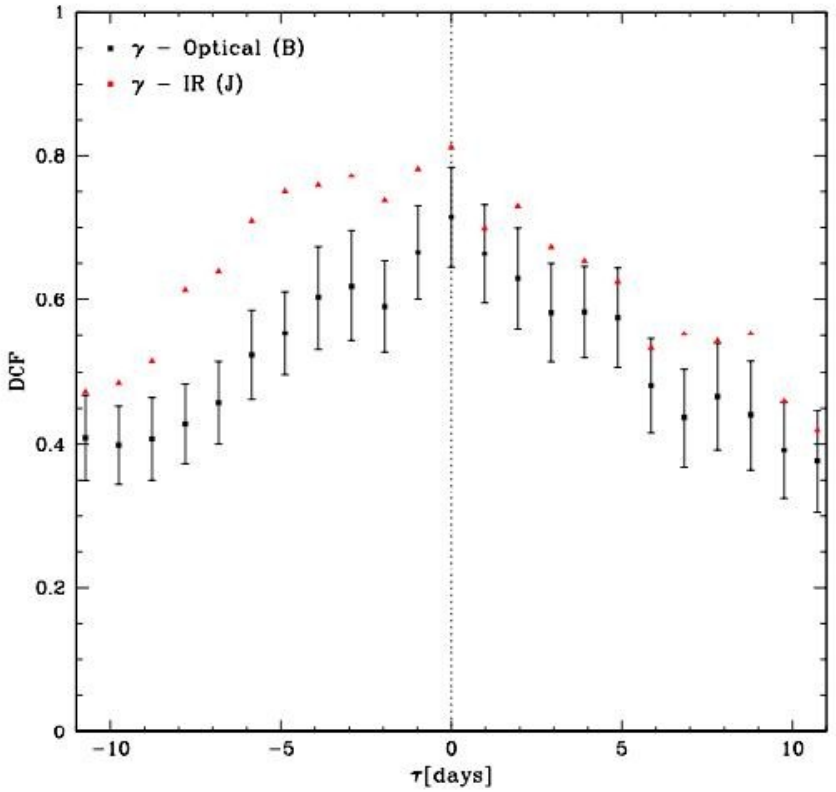

Discrete correlation function between optical (B-band, black squares), and infrared (J-band, red dots and similar error bars) vs. 0.1 – 300 GeV Fermi data. Data are consistent with **zero** delay between optical, IR, and γ-ray data but the J-band data suggest a delay of ~5 days.

(Figure 2, Bonning et al. 2008, ApJ (arXive:0812.4582v1)

Non-zero delay between 0.1-100 GeV (Fermi/LAT) and 15 Ghz VLBA emission from MOJAVE Project for 183 LAT-detected AGNs: γ-rays lead radio emission from 1.2 months in the source frame (Pushkaev, Kovalev, and Lister, 2010).

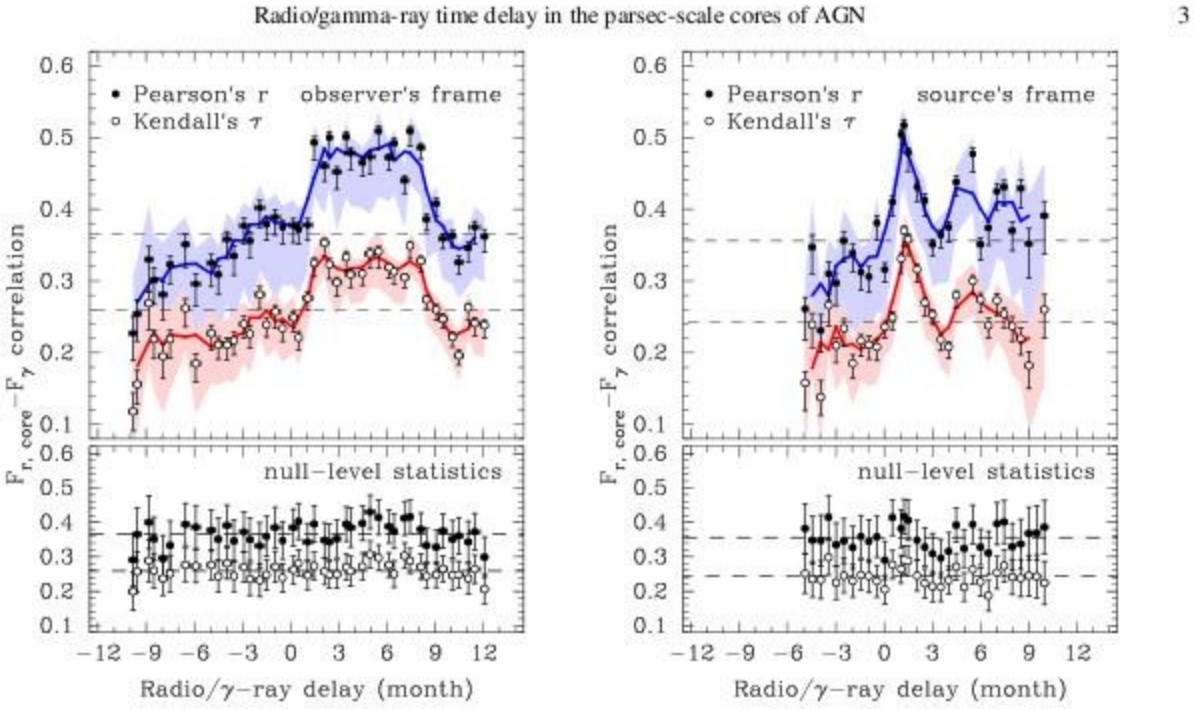

Figure 1. *Left:* Upper panel: flux-flux correlation level as a function of the time interval between integrated 0.1 – 100 GeV photon flux and radio core flux density measurements in the observer's frame. Filled circles represent the Pearson's r statistic, and open circles denote the Kendall's τ statistic. The error bars are shown at the 68% level, while shaded areas represent 95% confidence regions. The thick curves are constructed by applying a three point moving average. Dashed lines show the null-basis level of the correlation due to the overall γ-ray photon flux versus radio flux density correlation. Lower panel: estimation of the null level correlation obtained by shuffling γ-ray photon fluxes for every source and keeping radio flux densities the same. *Right:* same curves, corrected to the source rest frame. A sharp peak at a delay of ~ 1.2 months is detected.

"Concurrent, Multifrequency Observations"

Concurrent = within a window of time that is short compared to the expected time scales for variability of the object.

Multifrequency = some representation of the frequencies over which one expects the emission to occur.

Simultaneous = sampling at the Nyquist rate.

We often rely on **assumptions** about **relative intensities and variability of core versus jet luminosities** in our estimations of source fluxes without confirming this independently.

The definition of **concurrent** and **multifrequency** are made problematic by the different **resolutions** of the observatories:

radio data from VLBI is milliarcseconds

radio data from VLA in arcseconds

Hubble space telescope 0.1 arcseconds

ground based optical telescopes in arcseconds or tenths of arcseconds

optical and IR interferometers claim milliarcsecond resolution

Chandra x-ray detector has a resolution of 0.5 arcseconds

SWIFT x-ray telescope has a resolution of 18 arcseconds

γ-ray detectors (AGILE, INTEGRAL, SWIFT, and FERMI/GLAST) have resolutions of degrees to a few minutes.

HESS, Magic, Whipple, AUGER, and others have resolutions of order a few arcminutes.

GRS 1915+105 radio variability: The radio and infrared data for the microquasar, are consistent with van der Laan expansion.

SS433: Variable in both radio and x-ray.

Cen A radio and x-ray variability: Historical data not consistent with van der Laan expansion, most directly because of the second radio flare without a corresponding x-ray flare.

3C454.3 γ-ray, UV, IR, and optical, and Cen A radio and x-ray variability: Data are **not** consistent with simple models, such as van der Laan expansion from a single plasmon. We require some mechanism of accelerating or injecting new particles into the emitting region (see e.g., Jean-Philippe Lenain's 2011).

Hypothesis:

The jet plays a significant part in the overall emission from the source. The jet propagates outward from the accretion disk through an extremely complex environment, which can provide seed photons and ambient material with which the jet interacts.

Consider BL Lac:

Now possible to resolve structure of core vs. jet as they change over frequency and time using VLBI data:

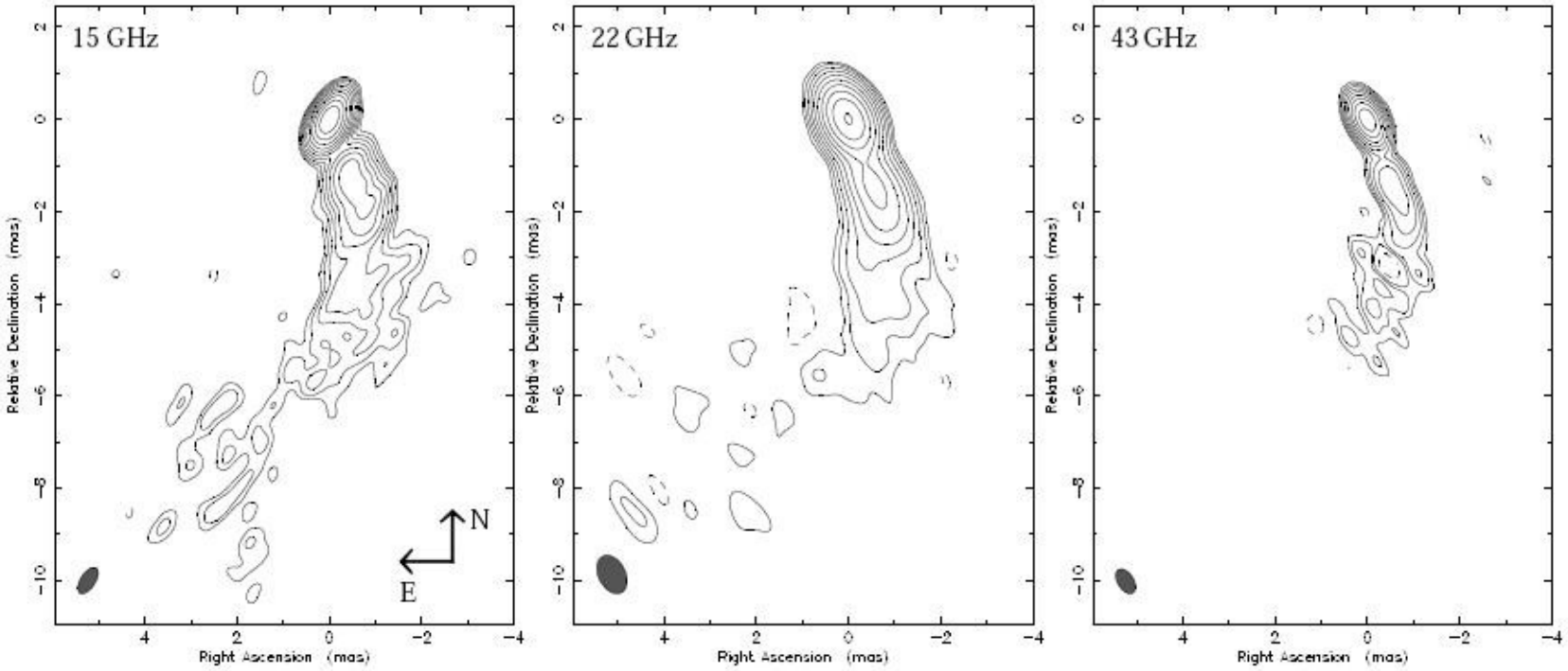

Fig. 1. VLBI images of BL Lac. **Left:** 15 GHz image (epoch 2002.03) with a beam of 0.64 mas × 0.32 mas at P.A. −33°. Peak flux density is 1.4 Jy/beam and contours start at 1.5 mJy/beam, increasing by a factor of 2. **Middle:** 22 GHz image (2002.05) with a beam of 0.88 mas × 0.58 mas at P.A. 27°. Peak flux density is 1.6 Jy/beam and contours start at 3 mJy/beam, increasing by a factor of 2. **Right:** 43 GHz image (2002.05) with a beam of 0.58 mas × 0.34 mas at P.A. 32°. Peak flux density is 1.3 Jy/beam and contours start at 3 mJy/beam, increasing by a factor of 2.

BL Lac radio variability and structure. Note estimates of core vs. jet flux in panel 3, which separates jets (e.g., jet 2 at 2 mas) from core.

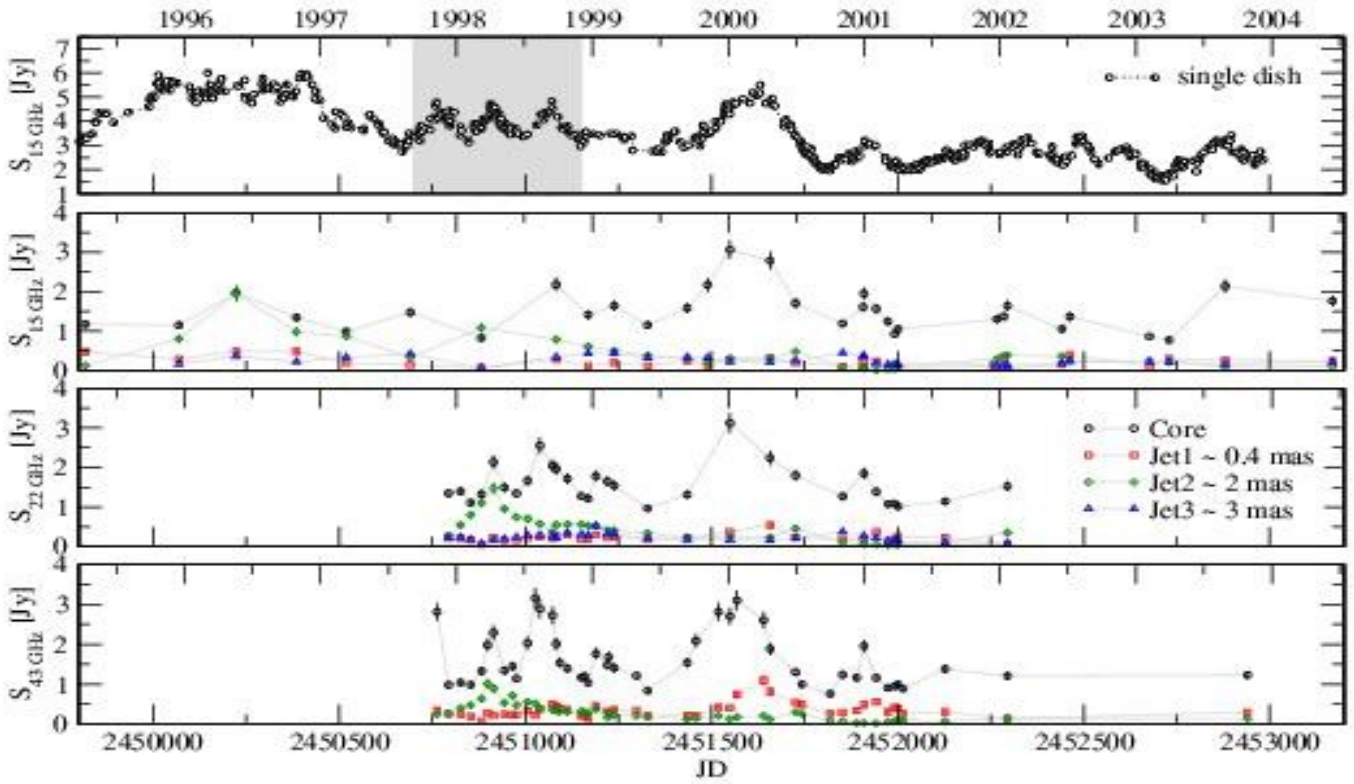

Fig. 3. Flux density evolution of different portions of the VLBI core-jet structure of BL Lac at 15 GHz, 22 GHz, and 43 GHz compared with the 15 GHz single-dish light curve. Different symbols denote different separation from the core r (see text for more details). The grey box highlights an example of a nice case study, where there are three equally bright flares, but the VLBI data reveals that contrary to the others the middle one was dominated by the jet and not by the core. Note that due to the rapid fading of the jet we do not show a Jet3 curve at 43 GHz.

Data from VLBA campaigns and MOJAVE (Monitoring **o**f **J**ets in **A**ctive galactic nuclei with **V**LBA **E**xperiments): A long-term monitoring program for monitoring AGN jets (see, e.g., Lister et al. arXiv:0902.2087v2, Ap.J.Letters, and Lister et al., 2009 AJ, 137, 3718). Note also x-ray optical jet pages on their website.

We have already seen movies of Sco X-1 and SS433.

What follows are "movies" of:

- **3C120** radio and x-ray from Marsher et al. (2009)
- **2251+158 (3C454.3**: concurrent optical, IR, UV, x-ray, and γ-ray observations from Bonning et al. 2009; apparent change in direction on parsec scales) -
- **1255+158.pol.mpg**
- **1308+326** (cone emission or precessing jet?)

3C120: Red ellipse represents inner accretion disk via Rossi XTE data, with insert showing x-ray light curve (see Marscher, 2003). Contours = 43 GHz intensity (VLBA). Inset: X-ray light curve (data courtesy of Alan Marscher and Jose-Luiz Gomez)1 mas = 0.70 pc @ D = 120 Mpc. (see Gomez et al. 2000 Science, 289, 2317)

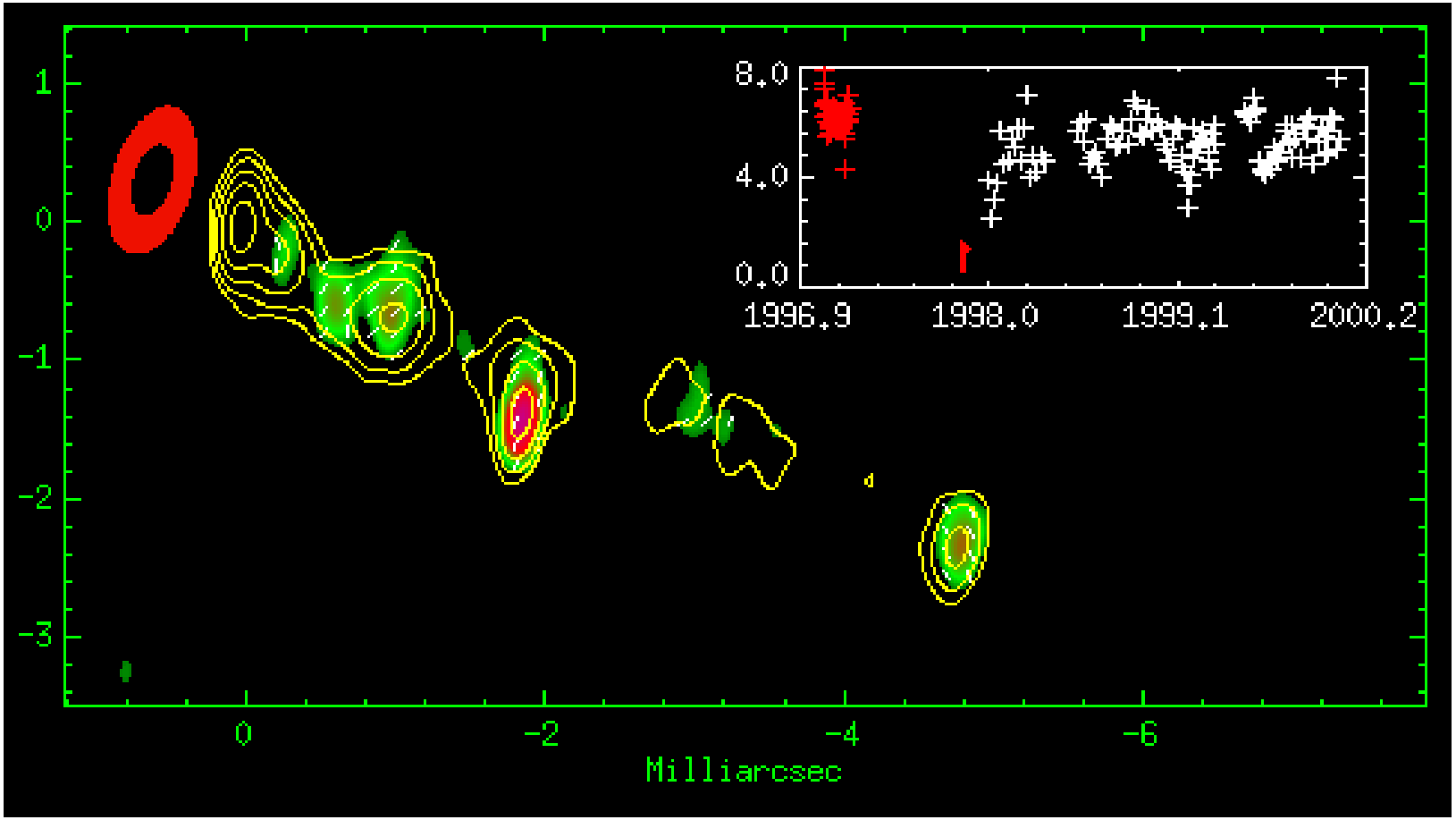

3c120 radio and x-ray variability

More complex structure of 2251+158(3C454.3), in VLBA at mas scales, from the MOJAVE Project (Lister et al. 1999)

Intensity and Polarization of 2251+156 (3C454.3) from VLBA (mas) scales.

Note the simple structure of (3C454.3) 2251+158, from VLA (arcsecond) scale data

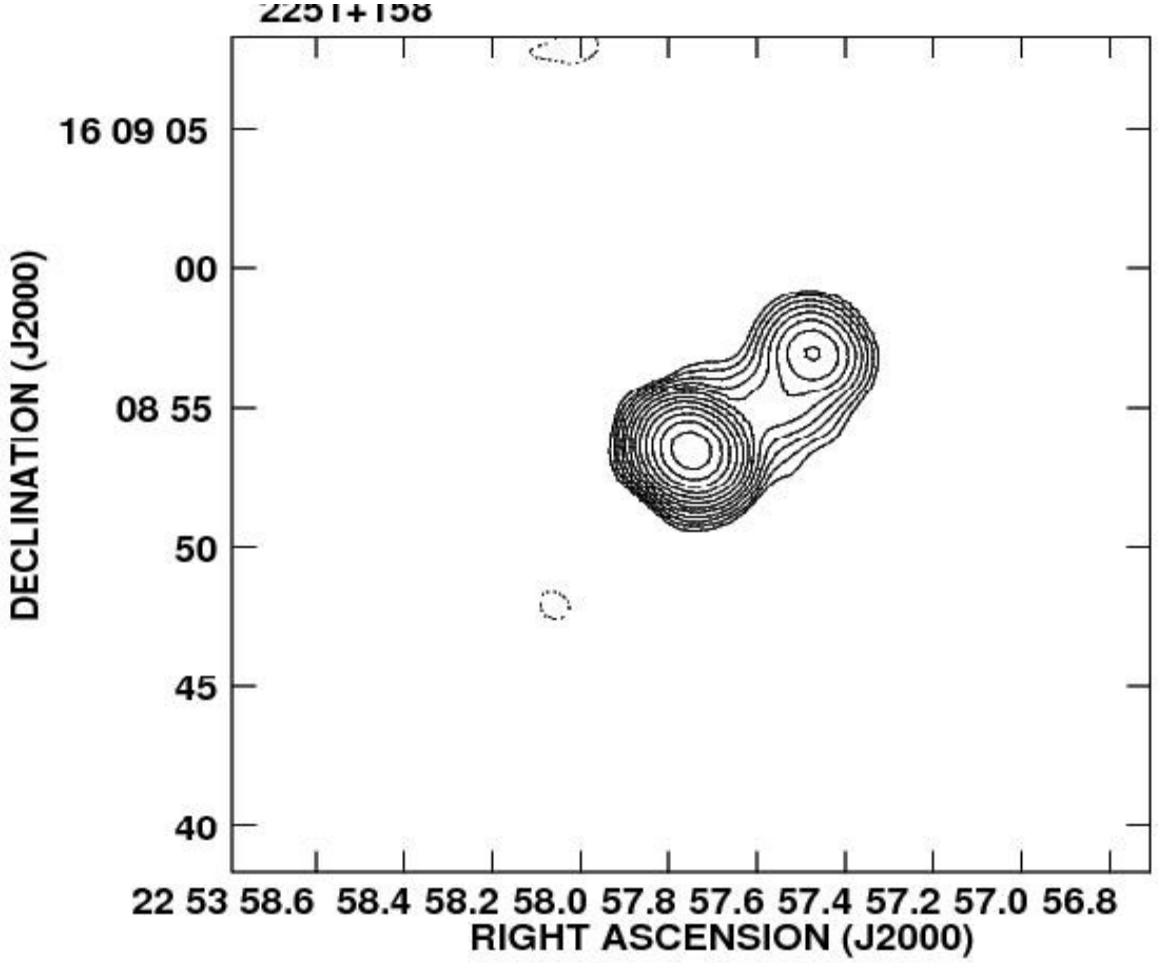

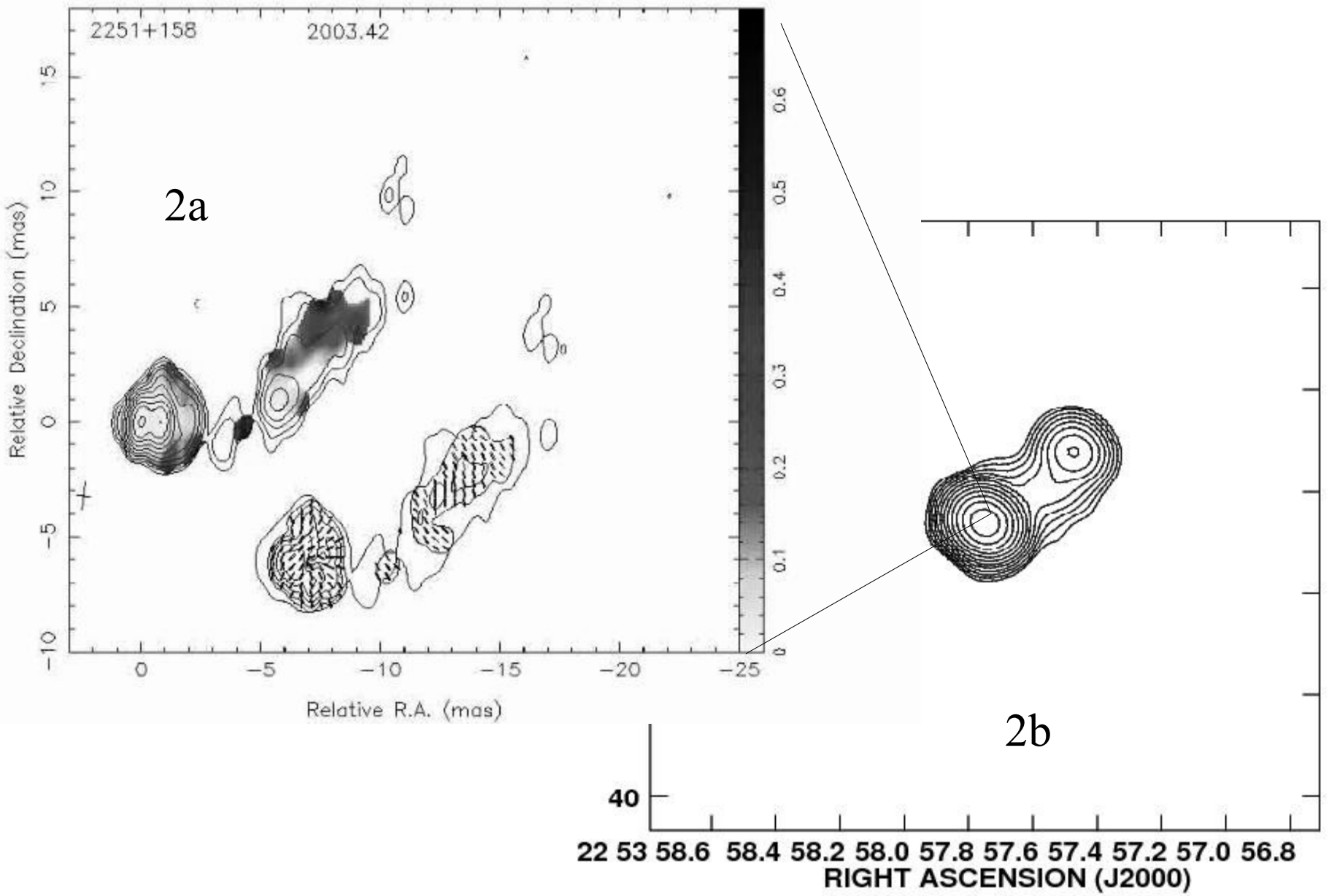
2251+158
2003.42
2a
Relative Declination (mas)
Relative R.A. (mas)
2b
40
22 53 58.6 58.4 58.2 58.0 57.8 57.6 57.4 57.2 57.0 56.8
RIGHT ASCENSION (J2000)

3C279 (1253-079) also has evidence for significant jet deflection

Possible precessing jet in 1308+326

VLBA observations of
QSO 1938+728 (z=0.302)

Chandra Image of MS0735.6+7421 Showing Cluster Holes

Jets can travel outward from the central engines of AGNs to distances > 100s of kiloparsecs.

In Cen A, the luminosity of the central engine, maintained over the propagation time scales of the jet required to form the giant radio lobes, can supply the energy of 10^{60} ergs that is present in those radio lobes (Beall and Rose, 1981).

It is possible that the cluster holes in this CHANDRA image of MS0735 +7421, have been formed by jets,

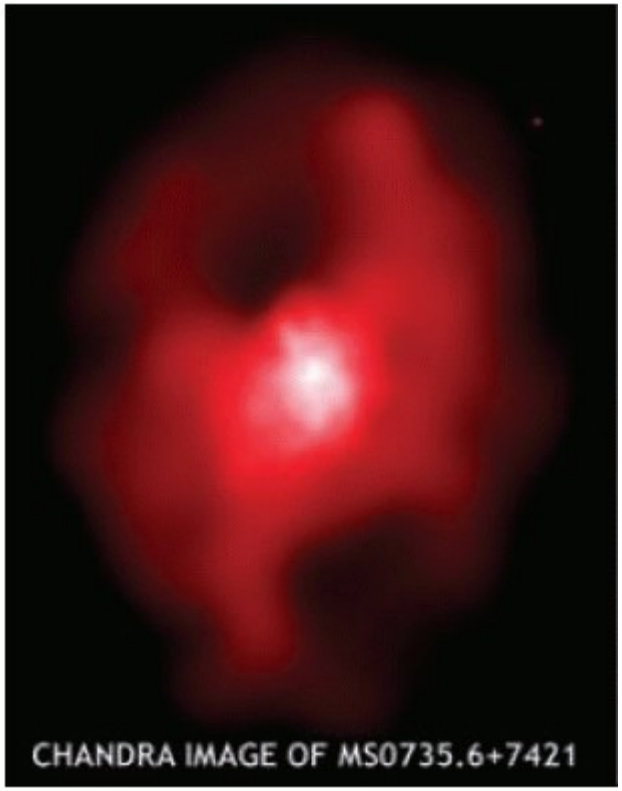

The environment that the jets propagate through is enormously complex.

The range of densities involved in the interaction varies over many orders of magnitude, and the jet itself clearly evolves by a number of mechanisms:

- Energy loss by various mechanisms
- Entrainment of the ambient medium contributes to the constitution of the jets, as does acceleration of particles.

The range of densities and scale lengths involved in the interaction varies over many orders of magnitude.

(see, e.g., Scott Holman, Ionson, and Papadopoulos, 1980 Ap.J. 239, 769, Rose, Guillory, Beall, and Kainer, 1984 Ap.J., 280, 550; and Beall 1980 in *Physical Processes in Hot Cosmic Plasmas*, Kluwer Pub.).

The environment that the jets propagate through is enormously complex (continued):.

This leads to an additional question: Are there **self-similar structures** at these different scales in individual jets and in galactic vs. extragalactic jets, and does that suggest an avenue for investigation? Of course this is precisely the point of Bozena Czerny's new project.

(see, e.g., Scott Holman, Ionson, and Papadopoulos, 1980 Ap.J. 239, 769, Rose, Guillory, Beall, and Kainer, 1984 Ap.J., 280, 550; and Beall 1980 in *Physical Processes in Hot Cosmic Plasmas*, Kluwer Publishers).

Polarization of some sources is consistent with a helical B-field around the jet. Bisnovatyi-Kogan, Romanova, and Lovelace (see, e.g., The 2001, 2005 and 2009 papers) have further developed their model of the jets' origins via twisted B-fields in accretion disks. This may provide a natural explanation for these helical B-fields that seem to be surrounding some jets.

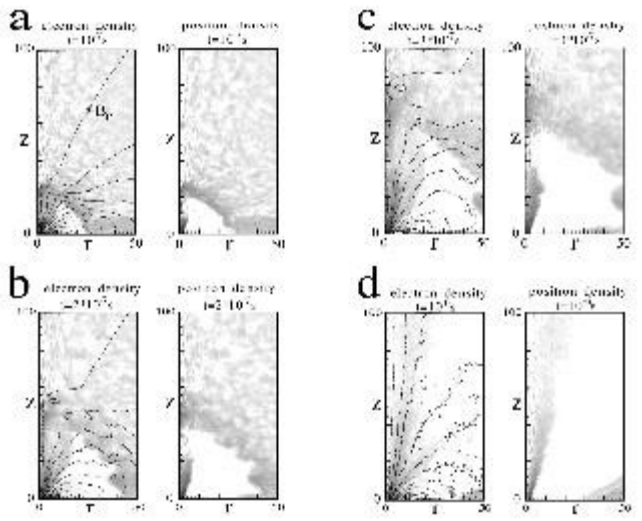

Fig. 4. Relativistic particle-in-cell simulations of the formation of a jet from a rotating disk. (a) -(c) give snapshots at times $(1, 2, 3) \times 10^{-7}$ s, and (d) is at $t = 10^{-6}$ s.

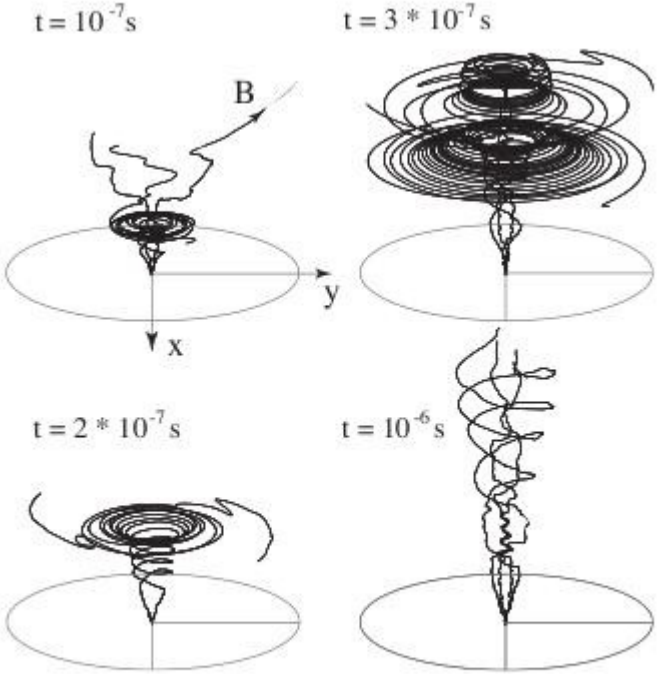

Fig. 5. Three dimensional magnetic field lines originating from the disk at $r = 1$, 2 m for the same case as Figure 4.

The model bears some similarities to the earlier work by W. Kundt and Gopal Krishna (J. Astrophys. Astr., 2004. 25. 115-127.

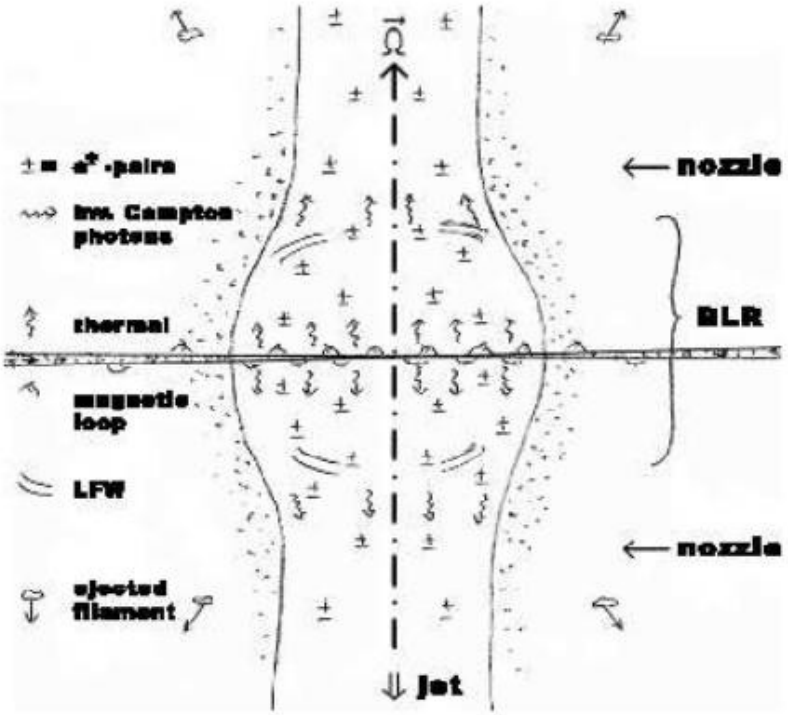

Figure 2: Sketch of a plausible Central Engine: Coronal Magnetic Reconnections create $e^{\pm}$-pairs, the warm Central (Star and/or) Disk emits photons, Low-Frequency Waves post-accelerate the escaping $e^{\pm}$, and the latter boost the thermal photons to high-energy γ-rays. An ambient thermal bulge serves as the deLaval nozzle from which a twin jet emerges, along the spin axis of the central rotator; in galactic-center sources, this region is observed as the BLR.

Energy available from accretion onto a compact object

Accretion onto a compact object represents the most plausible source for the power in many astrophysical settings, including AGN, because of the efficiency of the accretion process relative to the rest mass energy of the object. This is so, somewhat surprisingly, even though the nuclear force is the strongest force and gravity is the weakest. The kinetic luminosity released by accretion is

$$dE/dt \sim (GM(dm/dt))/r \tag{1}$$

where M is the mass of the compact object, G is the gravitational constant, dm/dt is the accretion rate, and r is the radius at which the energy is released.

The escape velocity, v, is related to the mass of the attracting body by the

$$(1/2)mv^2 \sim GMm/r, \tag{2}$$

and for a compact object, $v \sim c$, i.e., the speed of light. Therefore,

$$dE/dt \sim \eta(1/2)(dm/dt)c^2 \tag{3}$$

where η is an efficiency factor usually taken to be $\sim 10\%$, and c is the speed of light. The efficiency for nuclear reactions is $\sim 1\%$.

Of course, accretion-powered sources include astrophysical jets.

see, e.g., Beall, J.H., 2001, Proceedings of the Vulcano Workshop

Concluding remarks:

Our ability to test concurrent variability is still hindered by differing resolutions of the instruments involved in the measurements. But concurrent VLBA(+an arm in a Molnaya orbit, i.e., RADASTRON), and optical (using the VLT) at mas resolutions should give a window into the acceleration regions of the jet and its initial interactions with the ambient medium.

This will further our understanding of the physical structure and temporal evolution of jets and their relation to disks. The time lags between the x-ray dips and γ-ray flares in Cyg X-1and Cyg X-3 are similar to those in 3C120 and other sources, and seem to confirm the disk-jet connection.

Concluding remarks:

The structure of the jets must provide clues to origin of the very high gamma-rays that have been detected.

Whatever the original constitution of the jets when they are accelerated, it is likely that they suffer a cascade process in the accelerating region. Their ultimate constitution appears to be a combination of hadrons and leptons shrouded by a surrounding, complex ambient medium.

The hadrons seem inevitable based of G. Burbidge's original conjecture about the great propagation distances.

Thank you!

Hadronic-Jet-Ambient-Medium γ–ray Spectrum: fully anisotropic calculation

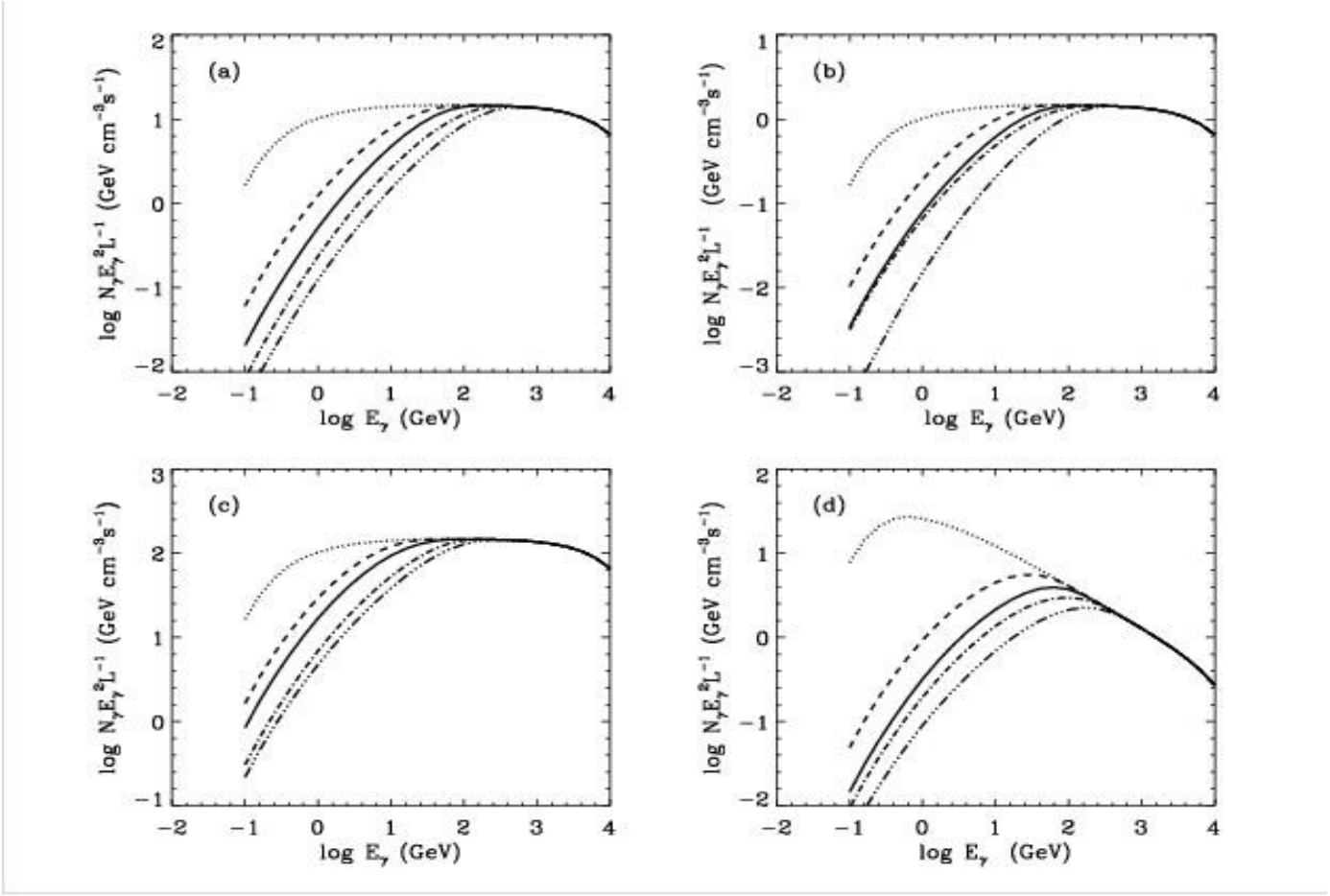

Beall and Bednarek, Ap.J.1999, 510, 188.

Complex environment for the Jets and the central engine of an AGN:

AGN Schematic showing the accretion torus with the Broad Line Region (BLR) clouds orbiting around the black hole and the accretion disk, the Narrow Line Region (NLR), and the jet of material propagating through central region and outward.

- Cen A core (below) from R. Kraft et al. 1999, 2000 Chandra observations.

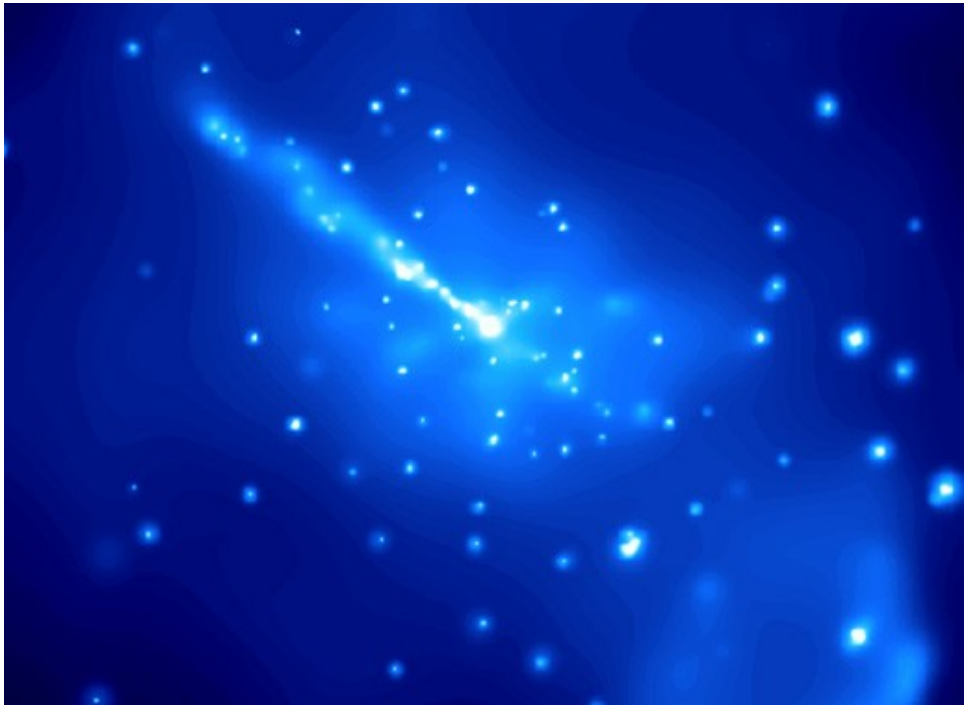

AGN schematic

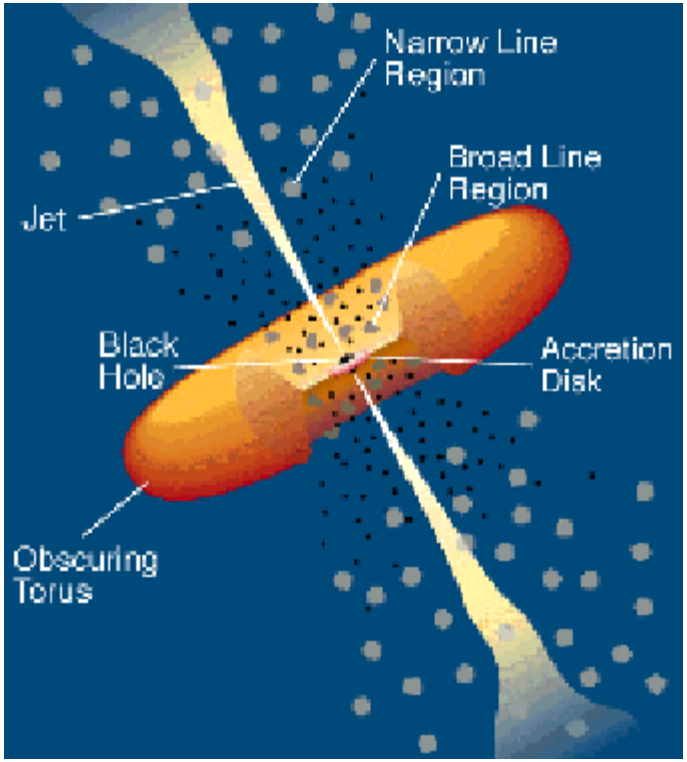

3C120: Red ellipse represents inner accretion disk via Rossi XTE data, with insert showing x-ray light curve (see Marscher, 2003). Contours = 43 GHz intensity (VLBA). Inset: X-ray light curve (data courtesy of Alan Marscher and Jose-Luiz Gomez)1 mas = 0.70 pc @ D = 120 Mpc. (see Gomez et al. 2000 Science, 289, 2317)

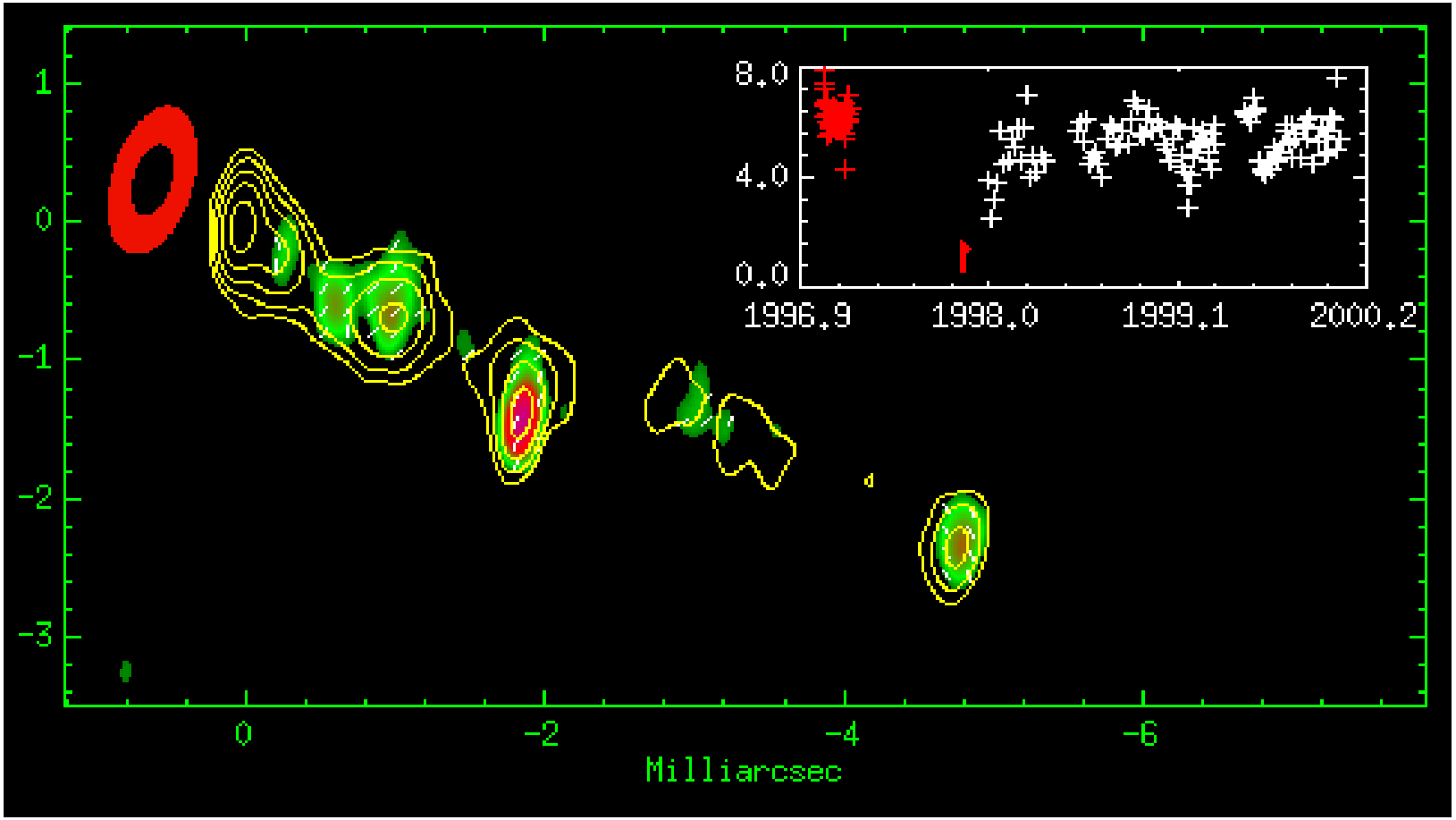

Radio interferometry using the VLBA:

The VLBA radio telescopes are located at:

* Mauna Kea, Hawaii (19°48′04.97″N, 155°27′19.81″W)
* Owens Valley, California (37°13′53.95″N, 118°16′37.37″W)
* Kitt Peak, Arizona (31°57′22.70″N, 111°36′44.72″W)
* Pie Town, New Mexico (34°18′03.61″N, 108°07′09.06″W)
* Los Alamos, New Mexico (35°46′30.45″N, 106°14′44.15″W)
* Fort Davis, Texas (30°38′06.11″N, 103°56′41.34″W)
* Brewster, Washington (48°07′52.42″N, 119°40′59.80″W)
* North Liberty, Iowa (41°46′17.13″N, 91°34′26.88″W)
* Hancock, New Hampshire (42°56′00.99″N, 71°59′11.69″W)
* St. Croix, United States Virgin Islands (17°45′23.68″N, 64°35′01.07″W)

Enhancement of VLBI using a satellite-based arm

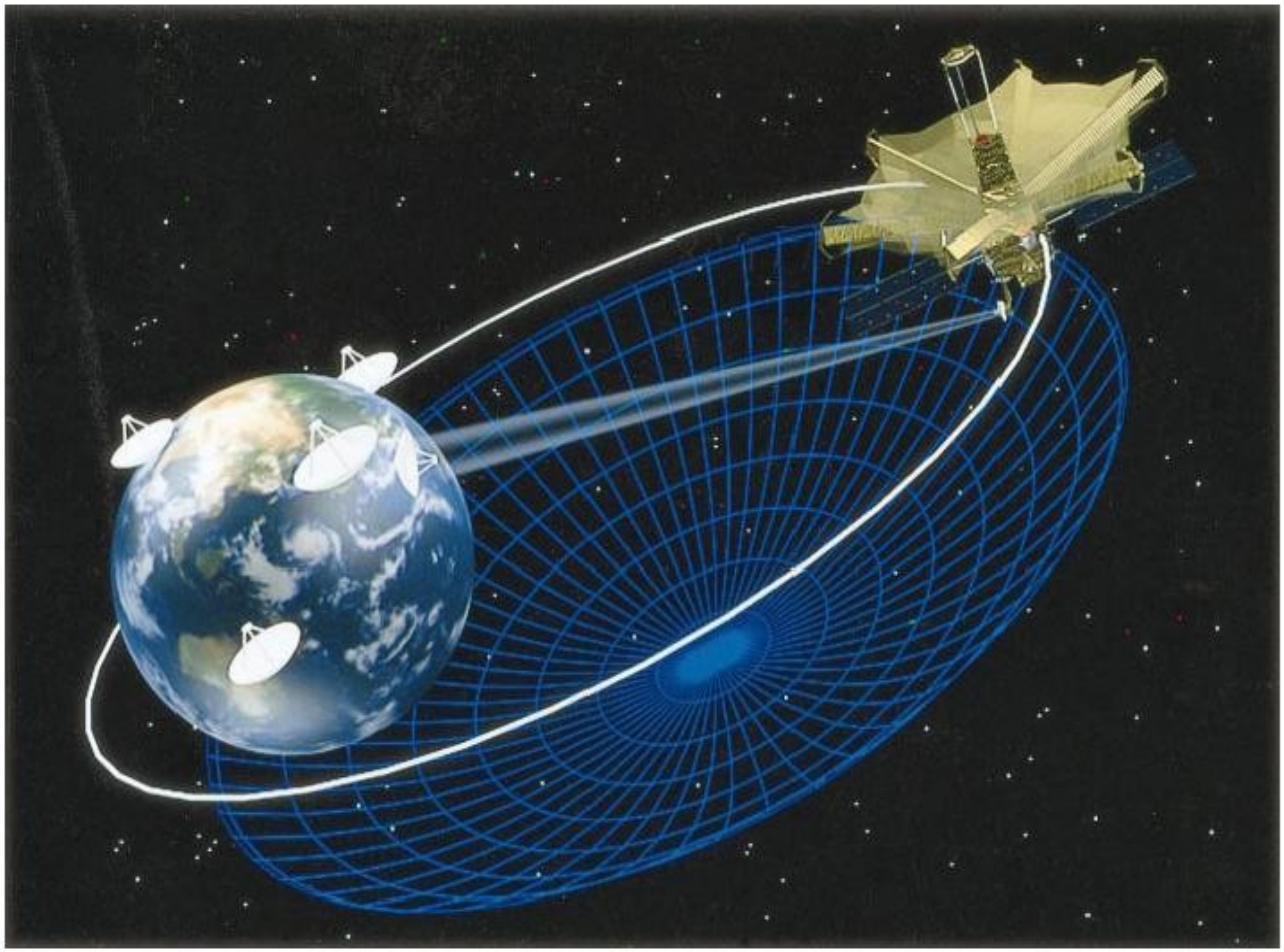

What are the limits of optical and IR resolutions? Optical and IR interferometry at the VLT:

The Very Large Telescope array (VLT) in Chile, consisting of four Unit Telescopes with main mirrors of 8.2m diameter and four movable 1.8m diameter Auxiliary Telescopes. The telescopes can work together, in groups of two or three, to form a giant 'interferometer', the ESO Very Large Telescope Interferometer.

But first, a reprise about van der Laan expansion

van der Laan

expansion:

radio flux time history

for a spherically

symmetric,

expanding synchrotron

source

(van der Laan, 1966)

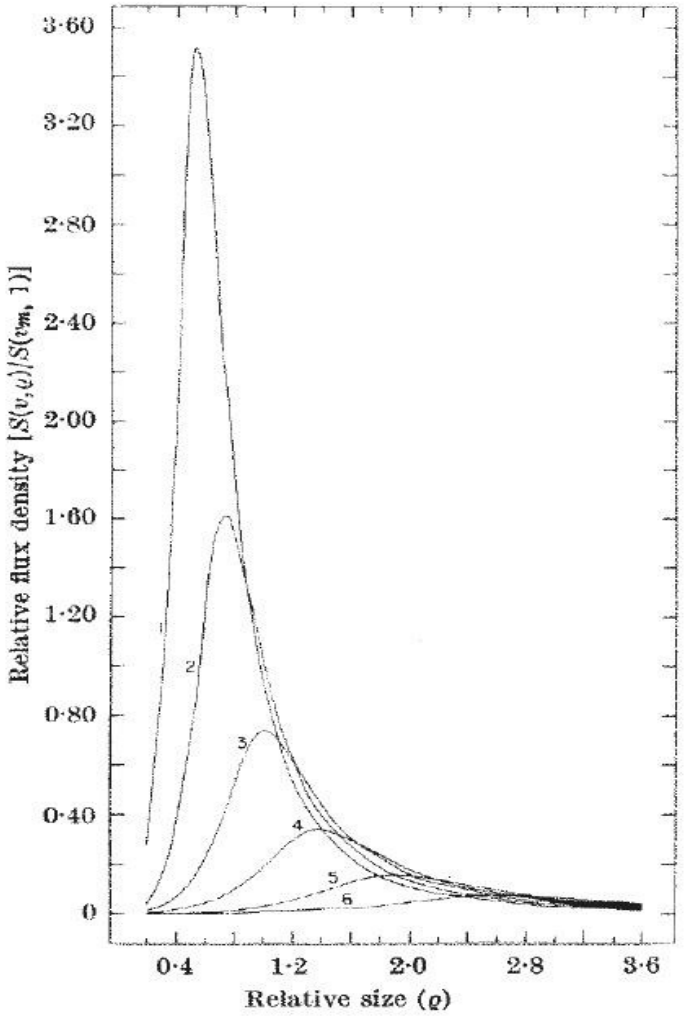

Fig. 1.—The radial dependence of flux density. The frequencies of successive curves differ by a factor of two. The spectral index (α) in this case is 0·25. Values for the various curves are $\nu m_0/\nu$: (1) 1/2; (2) 1; (3) 2; (4) 4; (5) 8; (6) 16.

van der Laan Expansion: successive plots show evolution of spectrum as the source expands

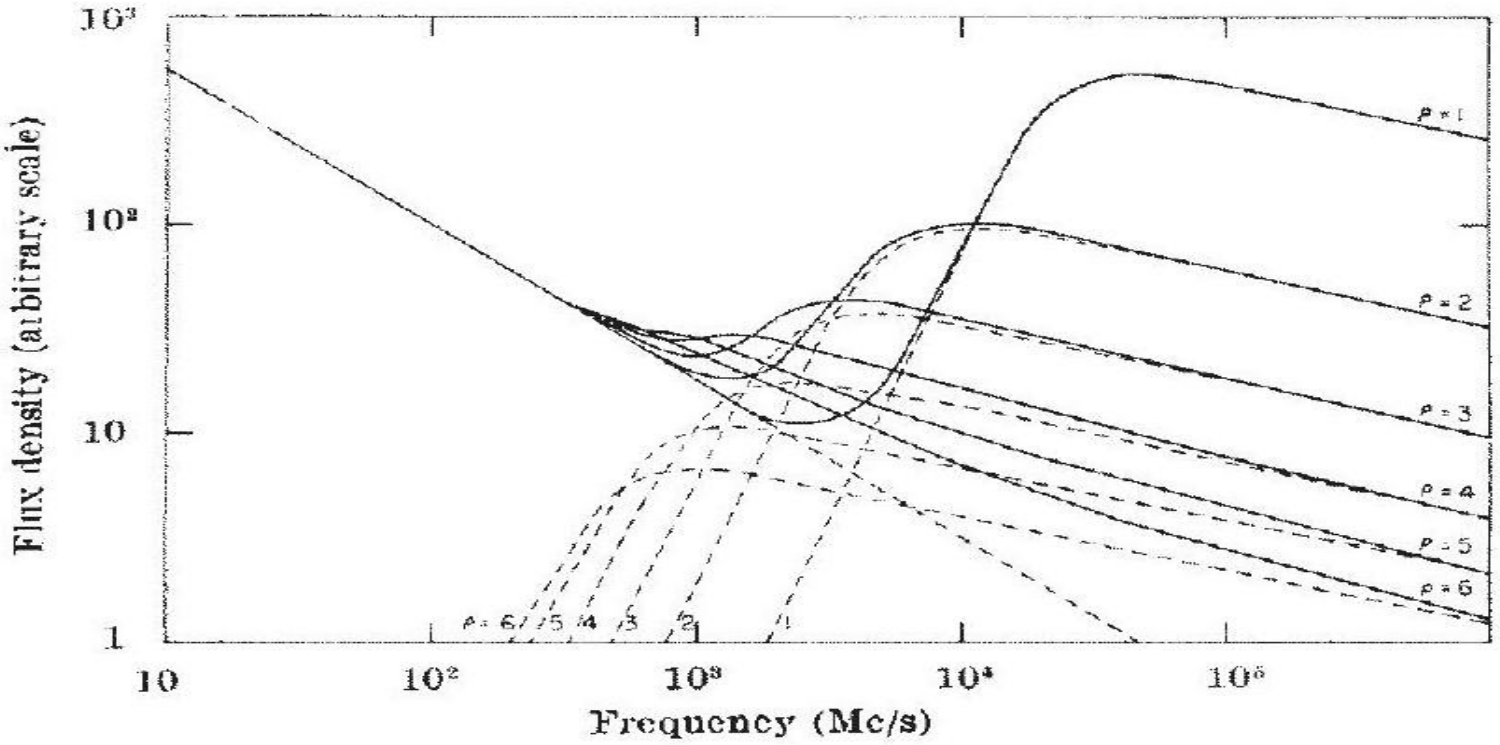

Fig. 2. The evolution of a typical variable radio source spectrum. The variable source spectrum is added to that of the constant source and the resultant is shown at successive integer values of ϱ.

Early Synchrotron Self-Compton model: a self-absorbed synchrotron radio spectrum + x-ray and γ-ray modelled by inverse-Compton processes can yield source parameters (see e.g., Grindlay 1975)

$$F_{ij} \propto \nu_c^{-(\Gamma_i - 1)/2}\, \theta^{-2}\, B^{-(\Gamma_i + 1)/2}$$

$$\times \int_{\nu_1}^{\nu_2} \nu^{[(\Gamma_i - 1)/2] - \Gamma_j - 1} F(\nu, \Gamma) d\nu\,, \qquad (1)$$

where $\nu_c = \gamma^2 \nu / [1 + (\gamma h \nu / m_0 c^2)]$, and $F(\nu, \Gamma)$ is given by Jones (1968). This formulism assumes spherical geometry of the source (though multiple components, either separate or concentric, can be included), as well as isotropic photon and electron distributions and magnetic field. The Compton-synchrotron flux thus depends on $\theta^{-2} B^{-(1+\alpha)}$.

(Grindlay, 1975 Ap.J.)

Synchrotron Self-Compton (continued):

If the synchrotron source is optically thick below a frequency ν_a where the flux is S_m, the magnetic field and angular diameter are related by (e.g., Kellermann and Pauliny-Toth 1969)

$$B = \nu_a^5(\theta^2/S_m)^2 1.62 \times 10^{-6} \text{ gauss (MHz, arcsec, Jy)} .$$

(Grindlay, 1975 Ap.J.)

In the SSC model, the spectrum of the IC photons mimics that of the original synchrotron spectrum.

This is also the case when the seed photons are thermal (blackbody) photons from interstellar clouds in AGN.

$$\frac{F(\nu_c)}{F(\nu_s)} = 2.47 \times 10^{-19}(5.25 \times 10^3)^q \times \frac{b(n)}{a(n)} T^{3+q} B^{-(q+1)} \left(\frac{\nu_c}{\nu_s}\right)^{-q}, \qquad (1)$$

where B is the magnetic field in gauss; $a(n)$ and $b(n)$ are determined from the synchrotron spectrum and depend only on the electron power-law index n; T is the temperature of the blackbody photon distribution in kelvins; and q is the spectral index of the X-ray energy spectrum [$q = (n - 1)/2$]. We choose $\nu_c = 2.4 \times 10^{19}$ Hz (100 keV) and $\nu_s = 5 \times 10^{10}$ Hz. Substituting these values and $q = 0.5$ obtained from the observations into equation (1) yields

$$\frac{F(\nu_c)}{F(\nu_s)} = 2.88 \times 10^{-19} T^{3.5} B^{-1.5}. \qquad (2)$$

Beall et al., 1978 Ap.J.

Modern SED modeled by SSC (Pian, 2007, Ghisillini 2003, Konopelko et al. 2003 Ap.J. 597,421), and Lenain (2010).

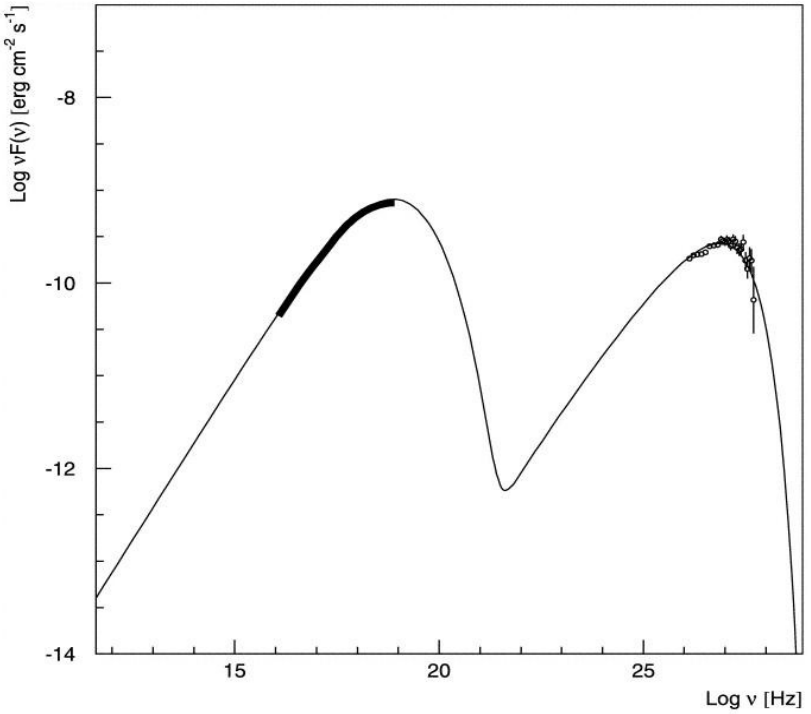

MKN 501

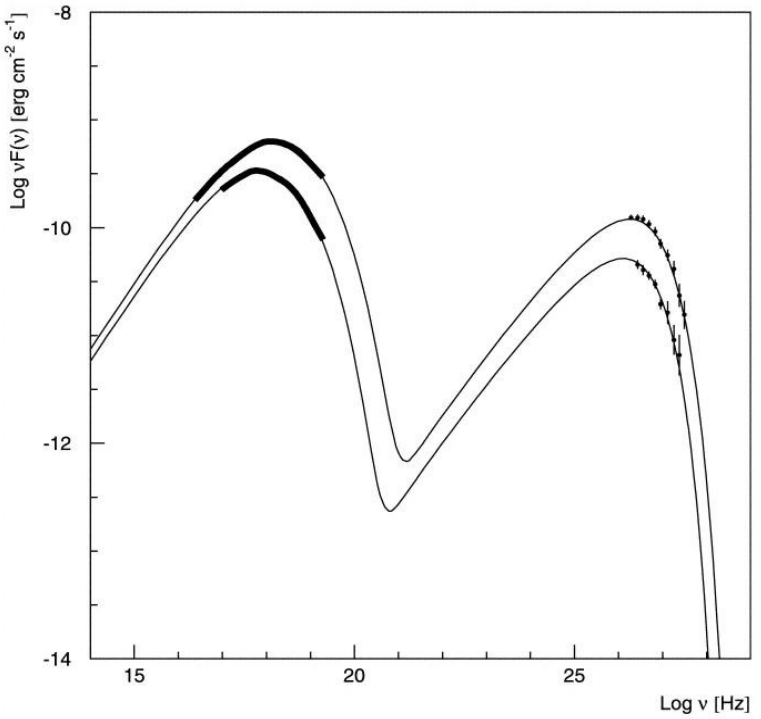

MKN 421